

000 JET EXPANSIONS: RESTRUCTURING LLM COMPUTA- 001 002 TION FOR MODEL INSPECTION 003 004

005 **Anonymous authors**

006 Paper under double-blind review

007 008 ABSTRACT 009

010 Large language models are becoming general knowledge engines for diverse ap-
011 plications. However, their computations are deeply entangled, resisting mod-
012 ularization which complicates interpretability, auditing, and long-term main-
013 tenance. We introduce JET EXPANSIONS, a framework for expanding recursive
014 residual computational graphs using jet operators that generalize truncated Tay-
015 lor series. Our method systematically decomposes language models into explicit
016 input→output computational paths and complementary remainders. This *func-*
017 *tional decomposition* provides a principled, knife-like operator for cutting through
018 entanglement in LLMs, enabling scalable model inspection. We demonstrate
019 how JET EXPANSIONS ground and subsume the popular interpretability technique
020 *Logit Lens*, reveal an ensemble of an exponential number of paths analytically ver-
021 ify prior research in a different branch and support several interpretability appli-
022 cations, including sketching a transformer language model with n -gram statistics
023 extracted from its computations and indexing model toxicity levels without cu-
024 rated benchmarks.

025 026 1 INTRODUCTION

027 The earlier wave of artificial intelligence (AI) featured symbolic systems, which store knowledge in
028 units, such as entities and relations. The latest advancement in AI, however, surfaces a largely *un-*
029 *structured* paradigm, particularly since the inception of large language models (LLMs) training with
030 massive unorganized web texts (Radford et al., 2019; Brown et al., 2020; Touvron et al., 2023a;b;
031 Rozière et al., 2024). Unlike symbolic AI, LLMs disperse knowledge across billions of entangled
032 parameters. This mismatch between *knowledge layout* and *computation layout* is at the heart of
033 LLMs’ opacity, seeding regulatory concerns about their security and maintainability. Once trained,
034 LLMs cannot be easily audited or updated. Removing toxic knowledge (Gehman et al., 2020), delet-
035 ing private information (Carlini et al., 2021), or incorporating new policies (Mitchell et al., 2021;
036 2022; Meng et al., 2022) is far from straightforward. In contrast, such operations could be trivial in
037 systems that structure knowledge into addressable units, as in symbolic AI. Therefore, this opacity
038 issue of LLMs fuels growing demands for interpretability, particularly in high-stakes domains such
039 as healthcare (Smith, 2021; He et al., 2025; Comeau et al., 2025) and robotics (Wachter et al., 2017;
040 Fernández-Becerra et al., 2024; Raptis et al., 2025).

041 Existing interpretability methods often take a *data-then-explanation* approach: curate inputs, hy-
042 pothesize which sub-computations matter, and observe activations to refine the hypothesis (Wang
043 et al., 2022; Meng et al., 2022; Goldowsky-Dill et al., 2023). But the real challenge is structural:
044 LLM computations are *entangled*, preventing us from isolating embedded knowledge into mean-
045 ingful units. While one can gain valuable insights with data-driven interpretability approaches, we
046 posit that the ability to reorganize computation into smaller, less entangled, end-to-end components
047 “systematically” – rather than “empirically” – is central to tackle such issue at scale.

048 We present JET EXPANSIONS, a principled, general-purpose framework for manipulating LLM
049 computations. Noting that LLMs are particular types of residual networks (He et al., 2016; Vaswani
050 et al., 2017), our key idea is to recursively expand residual computations using *jet operators* (Ehres-
051 mann, 1951), the functional counterpart of truncated Taylor series. This process yields functional
052 rewritings of the model into two parts: (i) explicit input→output polynomial functions, which we
053 call *jet paths*, and (ii) complementary nonlinear remainders. Crucially, JET EXPANSIONS operates

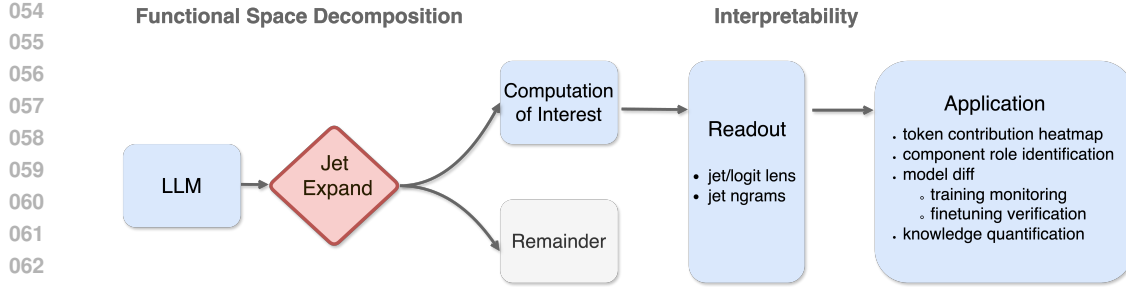


Figure 1: JET EXPANSIONS restructure residual computations into explicit input→output paths and a complementary remainder. From these paths we can extract logits, and n -grams without retraining or additional data. These readouts support downstream applications such as token contribution heatmaps, model comparison, training monitoring, and fine-tuning verification.

at a functional level, requiring no additional data, nor training. We show that JET EXPANSIONS encompass existing interpretability tools such as the Logit Lens (nostalgebraist, 2021b), and extend them to new instantiations such as extracting n -gram probability table from LLMs. This enables dataset-free, symbolic sketches of transformer LLMs and allow us to perform global interpretability studies. Figure 1 illustrates the pipeline.

We validate our framework through case studies across several autoregressive LLMs (*GPT*, *Llama*, *OLMo*). JET EXPANSIONS enable several empirical model inspection usages: i) understanding inner mechanisms via jet lens (Section 5.2.1); ii) assessing fine-tuning effects, e.g. quantifying toxicity levels with jet n -grams, showing RLHF alignment (Bai et al., 2022) reduces but does not eliminate toxic knowledge (Section 5.2.2); iii) analyzing pretraining dynamics, e.g. tracking how bi-grams such as “at least” are promoted then suppressed in *OLMo* (Section H). These results demonstrate that JET EXPANSIONS provide a powerful, dataset-free operator for restructuring LLM computations, paving the way for more transparent, interpretable, and maintainable foundation models.

Our contributions.

1. A new angle on interpretability: treating it as *function decomposition*, rather than input-driven attribution or circuit identification on particular datasets.
 2. A principled theoretical framework, based on jet operators, formally grounding existing tools such as *Logit Lens* (nostalggebraist, 2021b;a) and *path expansion* (Elhage et al., 2021).
 3. Preliminary but wide-ranging case studies, revealing insights into LLM internal mechanisms, fine-tuning knowledge shifts, and toxicity levels.

2 BACKGROUND AND PRELIMINARIES

Language models as residual networks. We focus on transformer language models (Vaswani et al., 2017), which are residual networks (He et al., 2016) consisting of L stacked residual blocks sandwiched between an encoder Enc and a decoder Dec. Formally, the full computation is

$$f = \text{Dec} \circ (\bigcirc_{\ell=1}^L (\text{id} + \gamma_\ell)) \circ \text{Enc}, \quad (1)$$

where γ_ℓ is the non-linear transformation in block ℓ . Unrolling the recursion, the hidden state after ℓ blocks is

$$h_\ell = h_0 + \sum_{j=1}^\ell \gamma_j \circ h_{j-1}, \quad h_0 = \text{Enc}(z). \quad (2)$$

This recursive form makes clear that residual links accumulate contributions from all preceding layers. We adopt the notion of *residual streams* (Elhage et al., 2021), where the computation of h_l can be viewed as nested terms entangling contributions across blocks (see also (Veit et al., 2016)). Table 1 summarizes the notation.

Taylor expansions and jets. To handle nonlinearities when restructuring residual computations, we turn to *jets* (Ehresmann, 1951), which generalize Taylor expansions. For $f \in C^{k+1}(\mathbb{R}^d, \mathbb{R}^d)$,

108 Taylor’s theorem at base point x_0 gives
 109

$$110 \quad f(x) = f(x_0) + \sum_{j=1}^k \frac{1}{j!} D^j f(x_0) (x - x_0)^{\otimes j} + O(\|x - x_0\|^{k+1}). \quad (3)$$

111 The k -th order *jet operator* abstracts this expansion as
 112

$$113 \quad J^k f: \mathbb{R}^d \rightarrow P^k, \quad J^k f(x_0)(x) = f(x_0) + \sum_{j=1}^k \frac{1}{j!} D^j f(x_0) (x - x_0)^{\otimes j}, \quad (4)$$

115 or equivalently, by leaving the polynomial action implicit,
 116

$$117 \quad J^k f(x_0) = f(x_0) + \sum_{j=1}^k \frac{1}{j!} D^j f(x_0).$$

118 Intuitively, $J^k f(x_0)$ captures the local structure of f up to order k , and we write $f(x) \approx_k$
 119 $J^k f(x_0)(x)$ to indicate agreement up to order k . Jets thus provide a principled operator for rewriting
 120 computations of f into decomposable pieces.
 121

122 *Remark 1* (Base points and variables as functions). When tracing back to the input $z \in \mathcal{X}$, base
 123 points x_0 and variables x may themselves depend on z . In that case, jets define maps $\mathcal{X} \rightarrow \mathcal{Y}$ via
 124 $J^k f(x_0(z))(x(z))$. For brevity, we often omit writing the variable x explicitly when clear from
 125 context. (See Appendix A for details.)
 126

127 Table 1: Summary of notation used in the paper.

Symbol	Meaning	Symbol	Meaning
\mathcal{X}	Input space	L	Depth (no. of blocks)
V	Vocabulary size	id	Identity map
$\mathcal{Y} = \mathbb{R}^V$	Output logits	U	Unembedding matrix
d	Hidden dimension	ν	Final normalization
$f: \mathcal{X} \rightarrow \mathcal{Y}$	Full network	h_ℓ	Hidden state at layer ℓ
$\text{Enc}: \mathcal{X} \rightarrow \mathbb{R}^d$	Encoder	β_ℓ	Residual block at layer ℓ
$\text{Dec}: \mathbb{R}^d \rightarrow \mathcal{Y}$	Decoder	γ_ℓ	Residual transform inside block ℓ
x_0	Base point (center)	x	Variable
$D^j f(x_0)$	j -th differential	$(x - x_0)^{\otimes j}$	j -fold tensor product
$J^k f(x_0)$	k -jet at x_0	$J^k f$	Jet operator
P^k	Degree- k polynomial space	w_i	Jet weight for i -th base point
ξ	Set of expanded terms	δ	Remainder of jet expansion

139 3 RELATED WORK

140 **Mechanistic interpretability and path rewriting.** A large body of work has sought to interpret
 141 the inner computations of large language models. One prominent category is *mechanistic interpretability* (MI) (Ferrando et al., 2024), which aims to reverse-engineer model computations by
 142 identifying, clustering, and labeling behaviors (Shah et al., 2024; Meng et al., 2022; Bricken et al.,
 143 2023) and attributing them to specific components, such as MLPs (Geva et al., 2021; 2022) or
 144 circuits (Conmy et al., 2023; Ferrando & Voita, 2024). However, these approaches often restrict analysis
 145 to atomic components (neurons, layers, or weights), which may not reveal the *full* mechanism of
 146 information processing. For example, Templeton et al. (2024) highlight the difficulty of drawing
 147 conclusions at the neuron level compared with higher-level feature representations, while Bolukbasi
 148 et al. (2021); Goldowsky-Dill et al. (2023) emphasize that many findings depend heavily on the
 149 chosen data distribution. A second category of approaches attempts explicit *path rewriting*. Veit et al.
 150 (2016) syntactically expand residual networks into exponentially many paths of varying length to
 151 study gradient behavior. Elhage et al. (2021) decompose one- and two-layer transformers into sums
 152 of uni-gram and bi-gram computation paths. Goldowsky-Dill et al. (2023) extend this line of work
 153 by developing path patching methods that aim to preserve functional faithfulness while isolating
 154 specific behaviors. Aligning with the second category, our approach manipulates functions directly
 155 rather than activations. It requires neither probe datasets (Belrose et al., 2023) nor sampling (Conmy
 156 et al., 2023; Ferrando & Voita, 2024; Voita et al., 2024). By allowing arbitrary portions of computation
 157 to be isolated from the monolithic transformer, JET EXPANSIONS abstract and generalize prior
 158 path-based characterizations (Veit et al., 2016; Elhage et al., 2021), where nonlinearities were often
 159 ignored or simplified (e.g. omitting layer norms, linearizing components, or implicitly assuming the
 160 nonlinear compositionality does not destroy the supposed independence of paths).
 161

162 **N-gram models as symbolic counterparts.** N-gram models, dating back to Shannon (1948),
 163 represent one of the earliest symbolic approaches to language modeling. They store explicit prob-
 164 abilities of token sequences, e.g. $\Pr(w_i \mid w_{i-1}, \dots, w_{i-n+1})$, in tabular form. This makes their
 165 *knowledge layout identical to their computation layout*: each symbol sequence has a directly ad-
 166 dressable probability entry. Such symbolic modularity enabled early successes in language mod-
 167 eling (Goodman, 2001) and tasks like machine translation (Brants et al., 2007). While later work
 168 combined n -grams with networks (Liu et al., 2024), recent studies revisit their role in relation to
 169 LLMs: analyzing the ability of transformers to simulate n -gram statistics (Svete & Cotterell, 2024)
 170 or measuring agreement between LLM predictions and n -gram rulesets (Nguyen, 2024). This re-
 171 newed attention motivates a direct bridge between n -grams and LLMs. JET EXPANSIONS provide
 172 this bridge, allowing corpus-free extraction of n -gram statistics *directly from LLMs* and thereby
 173 recovering a form of symbolic modularity within their entangled computations.

174 **Taylor expansions and jets.** Taylor expansions are ubiquitous tools in analyzing learning be-
 175 haviours (Jastrzebski et al., 2017), notably with linearization ($k = 1$). For example, Belrose et al.
 176 (2024) applied Taylor expansion on the loss to demonstrate the learning preference of neural net-
 177 works. Xu et al. (2022) used a second-order Taylor expansion over the data distribution to interpret
 178 optimal features. The generalized jet notions were introduced in machine learning in the context
 179 of automatic differentiation tools by Bettencourt et al. (2019), and is an experimental feature in Jax
 180 (Bradbury et al., 2018), but has been studied before (see e.g. Griewank & Walther, 2008). We lever-
 181 age jets not merely as approximation tools, but as operators to restructure residual computations in
 182 LLMs into explicit input→output paths and complementary remainders.

184 4 RESTRUCTURING LLM COMPUTATION WITH JET EXPANSIONS

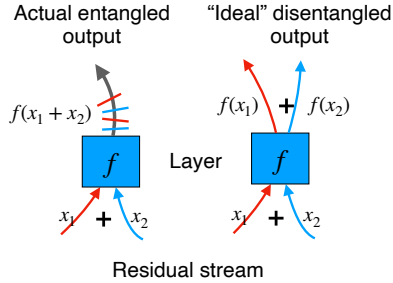
186 4.1 LINEAR CASE: EASY TO RESTRUCTURE

188 We begin with the linear case, where residual computations can be reorganized *exactly*. Assuming
 189 $\gamma_\ell(x) = A_\ell x$ for some $A_\ell \in \mathbb{R}^{d \times d}$, encoder $\text{Enc} = E$, and $\nu = \text{id}$, eq. (1) expands as follows

$$190 \quad f = \text{Dec} \circ \left(\bigcirc_{\ell=1}^L (\text{id} + \gamma_\ell) \right) \circ \text{Enc} = U \left(\sum_{S \subseteq 2^{[L]}} \prod_{\ell \in S} A_\ell \right) E = \sum_{S \subseteq 2^{[L]}} f_S, \quad (5)$$

192 where $2^{[L]}$ is the power set of $[L] = \{1, \dots, L\}$ and each path $f_S = U \left(\prod_{\ell \in S} A_\ell \right) E =$
 193 $U W_S E, W_\emptyset = I$, is itself a linear map from \mathcal{X} to \mathcal{Y} . Thus, the entire network can be written
 194 as the sum of 2^L explicit input→output paths f_S . This exact decomposition makes linear resid-
 195 ual networks intrinsically easy to restructure for interpretability because the output is a simple sum
 196 of its components: one can directly analyze the contribution of each path, study their interactions,
 197 and understand the global input→output relationships. In the nonlinear case, however, such a clean
 198 decomposition no longer holds, motivating the use of jets.

200 4.2 NONLINEAR CASE: JETS TO THE RESCUE



213 Figure 2: Convex combinations of jets
 214 disentangle a residual stream h_ℓ (a sum
 215 of terms) into sub-streams in function
 space, each isolated for further analysis.

201 $J^k f(x_0)$ encodes all information about a function f up to
 202 order- k derivatives at a base point x_0 , providing a vector-free
 203 representation of its local behavior. This makes jets a prin-
 204 cipled tool for reorganizing computations in LLMs. Lemma 1,
 205 proved in Appendix A, formalizes their *disentangling prop-
 206 erty*: a jet at a sum of inputs can be written as a convex com-
 207 bination of jets at individual inputs, up to higher-order error.
 208 This allows us to carve apart nested residual terms into sep-
 209 arate, analyzable contributions (Figure 2).

210 **Lemma 1** (Disentanglement of Jets). *Let $f \in C^\infty(\mathbb{R}^d, \mathbb{R}^d)$,
 211 $k \in \mathbb{N}$, $N \in \mathbb{N}^+$, $\{\textcolor{red}{x}_i\}_{i=1}^N$ be a set of jet base points, and $w \in$
 212 $\Delta^{N-1} \subset \mathbb{R}^N$ be a set of jet weights (i.e., $w_i \geq 0$, $\sum_i w_i =$
 213 1). Define the sum $\bar{x} = \sum_{i=1}^N x_i$ and $r = \max_i w_i \|x_i - \bar{x}\|$. Then the k -jet of f at the sum \bar{x} satisfies*

$$214 \quad J^k f \left(\sum_{i=1}^N \textcolor{red}{x}_i \right) = \sum_{i=1}^N w_i J^k f(\textcolor{red}{x}_i) + O(r^{k+1}).$$

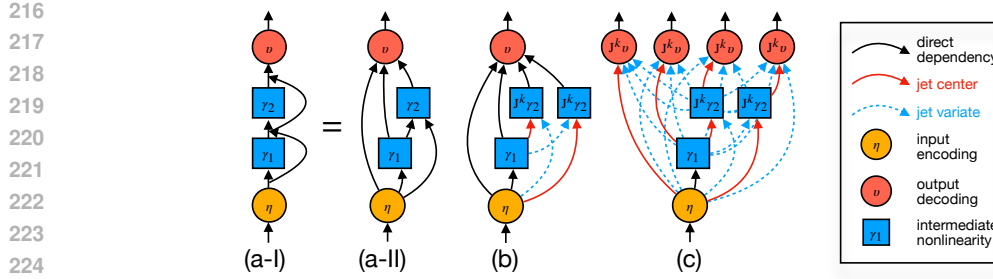


Figure 3: Carving a two-block network. (a) Nested entanglements. (b) Inner expansion at γ_2 . (c) Outer expansion at Dec, yielding 4 explicit paths.

*Example 1 (JET EXPANSIONS of **ReLU**).* Consider the **ReLU** activation function $\gamma : \mathbb{R} \rightarrow \mathbb{R}^+$ defined as $\gamma(x) = [x]_+$. For $x > 0$, $\gamma'(x) = 1$. For $x < 0$, $\gamma'(x) = 0$. Higher order derivatives are zero almost **everywhere**. If $x = x_1 + x_2$, then for almost every x , there exist $w \in \Delta^1$ such that

$$\gamma(\mathbf{x}_1 + \mathbf{x}_2) = w_1 \mathbf{J}^1 \gamma(\mathbf{x}_1)(\mathbf{x}) + w_2 \mathbf{J}^1 \gamma(\mathbf{x}_2)(\mathbf{x}) = w_1(\gamma(\mathbf{x}_1) + \gamma'(\mathbf{x}_1)x_2) + w_2(\gamma(\mathbf{x}_2) + \gamma'(\mathbf{x}_2)x_1).$$

In other words, for almost every **base point** $x = x_1 + x_2$, there exists a convex combinations of jets that **can recover the original function γ exactly**. Indeed, if either $x_1, x_2 > 0$ or $x_1, x_2 < 0$, then any convex combination is exact. If only one of the two terms is positive, say $x_1 > 0$ and $x_2 < 0$, then we can set $w_1 = 1$ if $x_1 + x_2 \geq 0$ and $w_1 = 0$ otherwise ($w_2 = 1 - w_1$). The specular argument applies for the case $x_1 < 0$ and $x_2 > 0$. From a global perspective, we can think of jet weights $w_i = w_i(x_1, x_2)$ as **optimizable** functions of x_1 and x_2 , rather than constants – and in the **ReLU** case, we obtain (almost everywhere) an exact first-order expansion. Conversely, one can see that the 0-th order JET EXPANSIONS of γ is not globally exact.

4.2.1 MOTIVATING EXAMPLE: CARVING A TWO-BLOCK RESIDUAL NETWORK.

Now we consider how to use jets to carve a typical computation graph. We begin with the simplest nontrivial case: a network with two residual blocks. Using Equation (1), its full computation is

$$f = \text{Dec} \circ \left(\underbrace{\text{Enc}}_{x_0} + \underbrace{\gamma_1 \circ \text{Enc}}_{x_1} + \underbrace{\gamma_2 \circ (\text{Enc} + \gamma_1 \circ \text{Enc})}_{x_2} \right).$$

The nested parentheses entangle contributions: the outer (purple) grouping mixes everything, while the inner (orange) ties γ_2 to both x_0 and x_1 . Traditional MI would select paths syntactically, akin to selecting modules in a PyTorch computation graph, ignoring these nesting effects. Jets let us cut both levels systematically and isolate the contributions of different input→output paths.

Step 1: Inner expansion. At γ_2 , taking $\{x_0, x_1\}$ as jet base points and using Lemma 1, the residual stream $x_2 = \gamma_2 \circ (x_0 + x_1)$ can be decomposed as

$$x_2 \approx_k \mathbf{J}^k \gamma_2(\mathbf{x}_0 + \mathbf{x}_1) = \underbrace{w_0 \mathbf{J}^k \gamma_2(\mathbf{x}_0)}_{x_{20}} + \underbrace{w_1 \mathbf{J}^k \gamma_2(\mathbf{x}_1)}_{x_{21}} + O(r^{k+1}),$$

so the original entangled stream x_2 separates into two sub-streams, as illustrated in Figure 3(b).

Step 2: Outer expansion. At Dec, the jet base points are updated from $\{x_0, x_1, x_2\}$ to $\{x_0, x_1, x_{20}, x_{21}\}$ after previous expansion. Using Lemma 1 and jet algebra (Proposition 1), yields

$$\begin{aligned} f \approx_k \mathbf{J}^k \text{Dec}(\mathbf{x}_0 + \mathbf{x}_1 + \mathbf{x}_{20} + \mathbf{x}_{21}) &= \underbrace{\bar{w}_0 \mathbf{J}^k (\text{Dec} \circ \text{Enc})}_{f_\emptyset} + \underbrace{\bar{w}_1 \mathbf{J}^k (\text{Dec} \circ \gamma_1 \circ \text{Enc})}_{f_{\{1\}}} \\ &+ \underbrace{\bar{w}_2 \mathbf{J}^k (\text{Dec} \circ (w_0 \mathbf{J}^k (\gamma_2 \circ \text{Enc})))}_{f_{\{2\}}} + \underbrace{\bar{w}_3 \mathbf{J}^k (\text{Dec} \circ (w_1 \mathbf{J}^k \gamma_2(\gamma_1 \circ \text{Enc})))}_{f_{\{1,2\}}} + O(r^{k+1}). \end{aligned}$$

corresponding to four distinct input→output paths $f_\emptyset, f_{\{1\}}, f_{\{2\}}, f_{\{1,2\}}$. This is shown in Figure 3(c). Each term aligns with what one might pick manually as a “path” in the network, but here it arises *systematically* from the JET EXPANSIONS.

270 The toy example above illustrates two key principles of our approach: recursive expansion of the
 271 nesting terms, and the use of disentangling property (Lemma 1) to isolate entangled contributions. In
 272 deeper networks with many blocks, however, manual expansion becomes infeasible. This motivates
 273 our general-purpose algorithmic framework, bringing such expansion to any depths.
 274

275 **4.3 GENERAL FRAMEWORK**
 276

277 Algorithm 1 describes the core operation of JET
 278 EXPANSIONS. At each block l , the algorithm
 279 applies Lemma 1 to a set of jet base points \mathcal{C} . For convenience, here $L + 1$ indicates the final
 280 decoder, Dec . The outputs are: (i) ξ , the set
 281 of polynomial terms (jet paths), where each term
 282 is the jet expansion centered at each $x_i \in \mathcal{C}$;
 283 and (ii) δ , a nonlinear remainder, collecting er-
 284 ror stemming from the Taylor expansion in Equa-
 285 tion (3) and error from Lemma 1. A key fea-
 286 ture is that jet base points can themselves be
 287 the outputs of earlier expansions. This enables
 288 recursive application of `jet_expand` through-
 289 out the network, unrolling the computation graph
 290 into end-to-end input→output paths. In partic-
 291 ular, when we apply `jet_expand` at the final de-
 292 coder layer $l = L + 1$, we obtain a functional
 293 rewriting of the model. Assume $(\xi_{L+1}, \delta_{L+1}) =$
 294 $\text{jet_expand}(f, L + 1, \mathcal{C}, k)$ for some choice of
 295 jet base points \mathcal{C} and order k , then

$$296 \quad f(x) = \sum_{e \in \xi_{L+1}} e(x, w) + \delta_{L+1}(x, w), \quad (6)$$

297 where the jet weights $w \in \Delta^{N-1}$ can be man-
 298 ually specified or optimized. Hence, recursive ap-
 299 plications of `jet_expand` yield a rewriting of the
 300 model as a sum of explicit paths, plus a comple-
 301 mentary remainder. Each path is an atomic unit
 302 of computation from input to output, mirroring the
 303 original function, but with simpler, additive struc-
 304 tures. This decomposition is purely algebraic and requires no extra data collection.

305 *Remark 2* (Jet weights). The jet weights w can be fixed, for example as $w_i = 1/N$, or optimized
 306 to minimize the remainder at a given x , such as in logit space. This optimization is efficient, as
 307 $\|U\delta_{L+1}(x, w)\|^2 = \|v(h_L(z)) - \sum_{e \in \xi_{L+1}} e(x, w)\|_{U^\top U}^2$, representing the squared distance between
 308 the expansion and the residual stream in \mathbb{R}^d , with the metric induced by U .

309 *Remark 3* (Remainders). Remainders generally do not vanish with increasing k , as the base points
 310 are user-defined. For linear residual networks, however, $\delta = 0$ for all $k \geq 1$, showing that Algo-
 311 rithm 1 exactly recovers the rewrite in Equation (5) for any w . In light of Equation (6), jet expansions
 312 should be viewed as algebraic rewrites of computational graphs, intended to aid interpretation rather
 313 than to minimize approximation error. In our experiments, δ is often small, and the cosine simi-
 314 larity between expanded and original logits approaches 1 (Figure 4, bottom). See App.B for detailed
 315 discussion.
 316

317 **Lemma 2.** *Residual nets with only ReLU nonlinearities admit exact first-order JET EXPANSIONS.*

318 **Runtime.** Evaluating ξ and δ at $x \in \mathcal{X}$ requires computing k th-order jets at cost $O(|\mathcal{C}|(F + kB))$, where F and B denote forward and backward passes of f . In practice, higher-order jets
 319 can be computed efficiently via recurrence relations and automatic differentiation primitives such
 320 as Jacobian-vector products (JVPs) (Griewank & Walther, 2008; Bettencourt et al., 2019). App.D
 321 reports empirical runtime scaling of our implementation.

Algorithm 1 `jet_expand`(f, l, \mathcal{C}, k)

Require: Net f as in eq. (1); block index $l \in [L + 1]$; jet base points $\mathcal{C} = \{\mathbf{x}_i\}_{i=1}^N$; jet
 order $k \in \mathbb{N}$
Ensure: Expanded polynomial terms ξ with
 weights w , and remainder δ

- 1: **if** $l \leq L$ **then**
- 2: **// residual block from f**
- 3: $\gamma_\ell \leftarrow f.\text{block}(l)$
- 4: **// residual block computation**
- 5: $h_\ell \leftarrow h_{\ell-1} + \gamma_\ell(h_{\ell-1})$
- 6: **// jet expansion at block l**
- 7: $\xi \leftarrow \{w_i J^k \gamma_\ell(\mathbf{x}_i)\}_{i=1}^N$
- 8: **// jet expansion at residual link**
- 9: $\xi \leftarrow \xi \cup \{w_i J^k \text{id}(\mathbf{x}_i)\}_{i=1}^N$
- 10: **// calculate remainder**
- 11: $\delta \leftarrow h_\ell - \sum_{e \in \xi} e$
- 12: **else**
- 13: **// jet expansion at decoder**
- 14: $\xi \leftarrow \{w_i J^k f.\text{Dec}(\mathbf{x}_i)\}_{i=1}^N$
- 15: $\delta \leftarrow f.\text{Dec}(h_L) - \sum_{e \in \xi} e$
- 16: **return** (ξ, δ)

324

5 APPLICATIONS OF JET EXPANSIONS

325

5.1 THEORETICAL APPLICATIONS

328 JET EXPANSIONS offer a principled framework that unifies and grounds existing techniques, such as
 329 *Logit Lens*, while enabling systematic derivations of new methods. Here we present several concrete
 330 instantiations of JET EXPANSIONS, and set the stage for the subsequent empirical studies.

331
 332 **(Super-)exponential expansion.** Algorithm 2 ex-
 333 tends our two-block example to arbitrary depth, pro-
 334 ducing 2^L paths via uniform jet weights. This mir-
 335 rors Veit et al. (2016)’s exponential view of resid-
 336 ual networks, but in an explicit and principled way.
 337 We defer the discussion on the connection between
 338 the expansion and the ensembling view on LLM
 339 computation to App.C. For $k \geq 1$, each polynomial
 340 term can be decomposed further by degree, isolating
 341 higher-order block interactions, hinting at a *super-*
 342 *exponential* ensemble perspective which we leave as
 343 future work.

344 **Jet lens and logit lens.** The *logit lens* (nostal-
 345 gicraist, 2021b; Geva et al., 2021; 2022; Merullo et al.,
 346 2023; Belrose et al., 2023) is a widely used mecha-
 347 nistic interpretability tool that applies the decoder to
 348 intermediate hidden states:

$$\text{LogitLens}_\ell(z) = U\nu(h_\ell(z)) = \text{Dec}(h_\ell(z)).$$

349 Aimed at highlighting the iterative refinement of the prediction across blocks, it is related to early
 350 exiting or early decoding in the context of conditional computation (see e.g. Panda et al., 2016;
 351 Elbayad et al., 2020; Geva et al., 2022). We can rewrite the logit lens with jet operator as follows

$$\text{LogitLens}_\ell(z) = \text{Dec}(h_\ell(z)) = J^0 \text{Dec}(\textcolor{red}{h_\ell(z)})(h_L(z)) = J^0_{\textcolor{red}{h_\ell(z)}} \text{Dec}(h_L(z)).$$

352 Here we retain the argument $h_L(z)$ to emphasize that the zeroth-order jet is applied within the full
 353 computation, as if the jet operator acts like a knife: slicing the network at layer ℓ and replacing
 354 the sliced computation with a truncated jet expansion. Indeed, $\text{Dec}(x) \approx_{k=0} J^0_{\textcolor{red}{h_\ell(z)}} \text{Dec}(x) =$
 355 $\text{Dec}(\textcolor{red}{h_\ell(z)})$, so the *logit lens* coincides with the zeroth-order jet of the decoder at the base
 356 point $h_\ell(z)$, equivalently $\text{jet_expand}(f, L+1, \{h_\ell\}, 0)$. This perspective suggests two di-
 357 rect generalizations of logit lens. First, *iterative jet lens* extends logit lens to higher-order jets:
 358 $\text{jet_expand}(f, L+1, \{h_\ell\}, k)$, $k \geq 1$. Second, *joint jet lens* expands with a broader set of base
 359 points rather than merely $\{h_\ell\}$: $\text{jet_expand}(f, L+1, \{\gamma_\ell \circ h_{\ell-1}\}_{\ell \in [L]}, k)$, thereby highlighting
 360 contributions of each block instead of the cumulative refinement of the residual stream.

361 **Jet n -grams.** n -gram statistics have gain their usage in analyzing LLMs (Elhage et al., 2021;
 362 Sverte & Cotterell, 2024; Nguyen, 2024), but existing methods rely on probing datasets. With JET
 363 EXPANSIONS, we can extract n -grams directly from the model. Concretely, since a model can
 364 be rewritten into a sum of polynomial terms or jet paths, we can select paths of interest, partic-
 365 ularly shorter ones, and evaluate them over the entire vocabulary space or its cartesian product to
 366 record the resulting logits. Formally, given a model’s expanded terms (jet paths) ξ , each path $e \in \xi$
 367 defines a function $e : \mathcal{X} = V^{n-1} \rightarrow \mathbb{R}^V$. The n -gram score for token i given a context x is
 368 $s(x)[i] = \sum_{e \in \xi} e(x)[i] / |\xi|$. By evaluating $s(x)$ for all $x \in V^{n-1}$, we obtain a complete n -gram
 369 table $(x, i, s(x)[i])$, $x \in V^{n-1}$, $i \in V$, where (x, i) identifies the n -gram and $s(x)[i]$ gives its score.

370 **From theory to applied.** The core expansion operator $\text{jet_expand}(f, \ell, C, k)$ has three key pa-
 371 rameters for a given model f : the *target block* ℓ , the *expansion center* C , and the *order* k . Together,
 372 they determine which portion of the residual computation f is carved out. Different choices of
 373 (ℓ, C, k) therefore yield different families of jet paths, and all empirical objects in our experiments
 374 correspond to evaluating such paths either *input-specifically* or *function-specifically*.

Algorithm 2 `exp_jet_expand(f, k)`

375 **Require:** Net f as in Equation (1); jet order
 376 $k \in \mathbb{N}$.
 377 **Ensure:** Expanded terms ξ (with uniform
 378 weights, $|\xi| = 2^L$) and remainder δ .
 379
 380 1: // initialize expansion
 381 2: $\xi \leftarrow \{f.\text{Enc}, \gamma_1 \circ f.\text{Enc}\}$
 382 3: **for** $\ell = 2$ to $L+1$ **do**
 383 4: $(\xi, \delta) \leftarrow \text{jet_expand}(f, \ell, \xi, k)$
 384
 385 5: // reweight terms uniformly
 386 6: $\xi \leftarrow \{e(\cdot, 1/|\xi|) \mid e \in \xi\}$
 387 7: $\delta \leftarrow f.\text{Dec}(h_L) - \sum_{e \in \xi} e$
 388 8: **return** (ξ, δ)

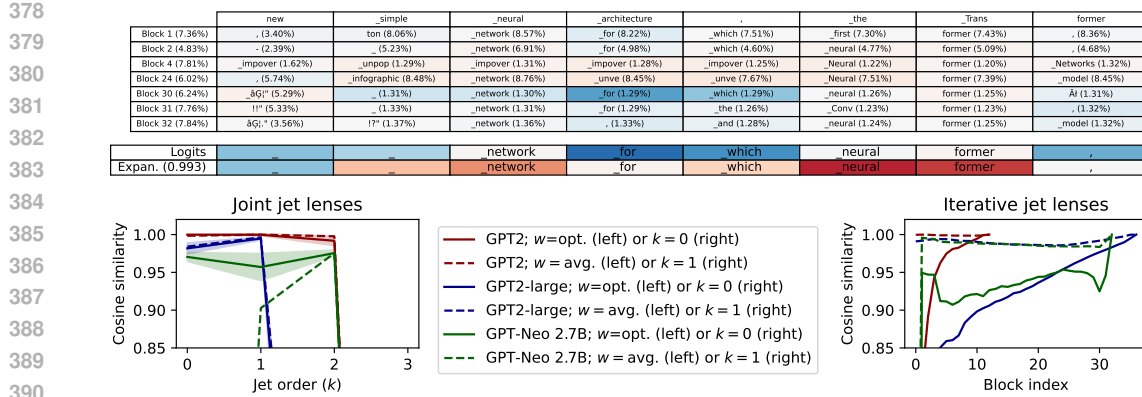


Figure 4: (Top) example of a joint jet lens on *GPT-Neo 2.7B* with $k = 1$, visualizing the seven blocks with highest average jet weights after optimization. Each table cell indicates the most likely token predicted by the jet path of each block. Optimized jet weight are displayed in the parenthesis next to the most likely token. We used a diverging blue-to-red color map tracking logit scores, centered at zero. The second table with two rows shows the model logits (Logits) and the expansion logits (Expan.), with cosine similarity (0.993) in parenthesis; in this case, all top-1 tokens perfectly coincide. (Bottom) plots of average cosine similarities between original and jet logits of joint (left) and iterative (right) lenses.

(i) **Input-specific.** For jet lenses (§5.2.1), we select expansion centers tied to a single input example (e.g. a sentence). When $\mathcal{C} = \{h_e\}$ and $k = 0$, the resulting decoder jet expansion recovers the classical *logit lens*. Using the same \mathcal{C} but $k > 0$ yields *iterative jet lenses*, which capture higher-order refinements of the residual stream. Expanding at the nonlinear outputs $\{\gamma_e(h_{e-1})\}$ with $k > 0$ produces *joint jet lenses*, decomposing the prediction into contributions from individual blocks.

(i) **Function-specific.** For jet n -grams (§5.2.2), we exploit a special property of LLMs: their inputs are provided by the token embedding function, which is itself part of the model, and thus can serve as a jet expansion center. Expanding at the embedding recenters the analysis on the *entire input space*, yielding jet paths over V^{n-1} and enabling a holistic, dataset-free characterization of the model’s global behavior tendency. In practice, bi-gram paths are obtained by: 1) expanding at Enc, 2) progressively adding $\text{MLP} \circ \text{Enc}$ as additional expansion centers, and 3) performing a final expansion at the decoder (See Alg.3 in App.E). The resulting low-arity paths $e : V^1 \rightarrow \mathbb{R}^V$ can be evaluated exhaustively, producing complete tables of *jet bi-grams* $(x_t, x_{t+1}, e(x_t)[x_{t+1}])$. These symbolic tables support global, dataset-free analyses: (i) *top- K scoring bi-grams*, which reveal broad behavioral tendencies of the model, and (ii) *keyword-conditioned bi-gram mass*, which aggregates scores over bi-grams associated with a semantic category (e.g., toxicity), providing a scalar indicator of how much such knowledge is embedded in the model.

Across both the input-specific (jet lenses) and function-specific (jet n -grams) settings, the connection to theory is direct: *each empirical quantity is simply a jet path evaluated on its natural domain*, with (ℓ, \mathcal{C}, k) translating theoretical choices into concrete experimental readouts.

5.2 EMPIRICAL CASE STUDIES

Setup. Experiments are done with open-source LLMs including *GPT-2* (Radford et al., 2019), *GPT-Neo* (Black et al., 2021), *Llama* (Touvron et al., 2023a;b; Rozière et al., 2024), and *OLMo* (Groeneveld et al., 2024). Experiments on jet n -grams were run on 128-CPU servers with 1TB memory, while those on jet lenses were computed on a single laptop CPU. In jet lens, jet weights w were optimized by gradient descent; for n -grams we restrict to zeroth-order jets from the jet paths of embedding \rightarrow MLP \rightarrow unembedding with uniform weighting. Algorithmic details and evaluation metrics are given in App.E and App.F.

5.2.1 CASE 1: ANALYZING LLM INNER WORKING

Jet lens. We use *jet lens* to analyze LLMs’ mechanisms when processing individual examples. Figure 4 (top) visualize a joint jet lens for *GPT-Neo-2.7B* (Black et al., 2021). For space reason, other examples are deferred to App.G.1. The first column

432 Table 2: MLPs in *OLMo-7B* and *Llama-2-7B* performing certain linguistic functions based on jet bi-grams
 433 extracted from the corresponding jet paths.

MLP Index	<i>OLMo-7B</i>					<i>Llama-2-7B</i>			
	1	3	9	17	19	6	7	18	19
Linguistic Role	-ly	-ing	-t	-than	-s	-ing	-es	-ing	-ly
Δ Logit Intervened	-4.19	-0.58	-9.73	-4.26	-7.42	-14.61	-3.55	-9.69	-11.93

434
 435 indicates the blocks. Here, a block, e.g. Block 1, contains one self-attention and one MLP module.
 436 All table cells depict top-1 tokens for the corresponding path through the particular block, following
 437 conventions from prior work (Belrose et al., 2023). We observe that the joint jet lens captures the
 438 synergy among different blocks, as the model prediction is decomposed into the contributions of
 439 several jet paths. Optimized jet weights are reported in the percentages.
 440

441 In this sense, *jet lens* with $k > 0$ may serve as tools to systematically discover such synergic be-
 442 haviors. We also find that higher-orders ($k > 0$) help iterative lenses deliver more meaningful
 443 interpretations than the *logit lens* ($k = 0$) for *GPT-Neo-2.7B* (see Figures 7 to 9). This is potentially
 444 due to their capability to trace indirect impacts of early layers on the final logits, which are otherwise
 445 missing under *logit lens*. Our findings are consistent with nostalgebraist (2021a); Cancedda (2024)
 446 where naive implementations of logit lens are shown to fail on *GPT-Neo* model family. Figure 4
 447 (bottom) present mean cosine similarities of joint and iterative jet lenses with respect to model out-
 448 puts for various *GPT* models and orders, averaged over 100 example sentences. The similarities are
 449 high and close to 1 for various k , showing however different behavior across model families and
 450 sizes. This indicates JET EXPANSIONS highly correlate with model outputs. In particular, the right
 451 plot compares the similarities of the logits obtained through iterative jet lenses for $k = 0$ (solid, line,
 452 the same as LogitLens) and for $k = 1$ (dashed lines), indicating an higher correlation of the latter
 453 with model outputs, potentially providing more faithful interpretations.
 454

455 **Jet paths of individual components.** By examining the representative jet bi-grams captured by
 456 jet paths of individual components, we can analyze their roles. In our case, we find some MLPs
 457 perform special linguistic functions. For example, in *OLMo-7B*, the jet path which passes through
 458 the 3rd MLP promotes the addition of the “-ing” suffixes to the current token. Similar MLPs with
 459 certain linguistic functions are listed in Table 2, where the negative Δ logit indicates removing the
 460 corresponding MLP harms the fulfillment of the particular linguistic functions. Note that the rela-
 461 tionships between functions and components are not necessarily one-to-one mappings. Particularly
 462 paths through multiple MLPs might work together to complete one linguistic function e.g. MLP 6
 463 and MLP 18 in *Llama-2-7B* can add “-ing” suffix. This echos work on circuit discovery (Elhage
 464 et al., 2022; Conmy et al., 2023; Ferrando & Voita, 2024), where the role of each component cannot
 465 be easily dissected and multiple components collaborate. Similar studies on the roles of attention
 466 heads can be found in App.G.2.
 467

468 5.2.2 CASE 2: ASSESSING FINE-TUNING EFFECT

469 Fine-tuning steers an LLM from pretraining’s vastness towards focused, task-specific intent. These
 470 shifts ripple distributedly across high-dimensional parameter space, often escaping full capture with-
 471 out extensive benchmarking. Jet n -grams, however, render the changes legible directly from the
 472 weights, revealing model differences through their n -gram “differing”.

473 **Code fine-tuning.** Comparing *Llama-2-7B* with its code fine-tuned variants, *CodeLlama*, reveals
 474 that differencing jet bi-grams highlights *code-specific* patterns such as `**kwargs` or `Assertion` (Table 3),
 475 confirming the acquisition of programming knowledge. This suggests that jet bi-grams can serve as
 476 a practical tool to verify if fine-tuning effectively imparts knowledge in target domains.

477 **RLHF alignment.** While *ToxiGen* scores suggest detoxification of LLAMA-2-7B-CHAT, jet bi-
 478 gram masses remain nearly unchanged (Table 4), indicating toxic associations persist in latent form.
 479 Challenging prompts from RealToxicityPrompts (Gehman et al., 2020) confirm that these associa-
 480 tions can still be triggered. Thus, RLHF appears to mask rather than erase toxic knowledge, a finding
 481 revealed directly by data-free jet bi-gram indices. This showcases a potential application of jet bi-
 482

486
 487 Table 3: Bi-grams before and after code fine-tuning. For brevity, we show every 50th bi-gram among the top
 488 1000. Bi-grams relevant to coding, such as `**kwargs` (a Python keyword), are **highlighted**. This demonstrates
 489 that our method can extract representative bi-grams reflecting fine-tuning quality.

Rank	Llama-2-7B	Codellama-7B	Codellama-Python-7B
0	(.more, _than)	(.like, wise)	(.like, wise)
50	(.Now, here)	(.just, ification)	(.like, wise)
100	(.system, atically)	(.in, _case)	(.all, udes)
150	(.all, erg)	(.get, ters)	(.no, isy)
200	(.on, ions)	(któber, s)	(output, ted)
300	(.other, world)	(.all, ud)	(Object, ive)
350	(.Just, ified)	(gebiert, s)	(.as, cii)
400	(.trust, ees)	(.Protest, s)	(.can, nab)
450	(.at, he)	(.deploy, ment)	(.transport, ation)
500	(.book, mark)	(Class, room)	(Tag, ging)
550	(.from, 而)	(.access, ory)	(.personal, ized)
600	(.WHEN, ever)	(.In, variant)	(.excess, ive)
650	(.where, about)	(.I, _am)	(.Add, itional)
700	(ag, ged)	(add, itionally)	(.**, kwargs)
750	(.he, he)	(.invalid, ate)	(name, plates)
800	(.all, anto)	(div, ision)	(.select, ive)
850	(.Tom, orrow)	(.process, ors)	(.Assert, ions)
900	(.for, ays)	(.Program, me)	(blog, ger)
950	(.Bach, elor)	(.set, up)	(.can, cellation)

503
 504 Table 4: Toxicity indexes for *Llama-2-7B* and *Llama-2-7B-chat* using different methods: *ToxiGen*, jet bi-
 505 grams, and *RealToxicityPrompts* challenge prompting. Higher numbers indicate higher toxicity scores on the
 506 corresponding benchmarks and higher toxic knowledge possession for jet bi-grams.

	ToxiGen Score	Jet Bi-grams Hartvigsen et al. (2022)	RTP Challenging Prompts			
			No	Very mild	Medium	Hard
<i>Llama-2-7B</i>	21.25	0.03445	38%	49%	64%	88%
<i>Llama-2-7B-chat</i>	0.0	0.03377	23%	35%	64%	84%

511 grams in constructing *data-free* indices that reveal embedded knowledge, offering complimentary
 512 views beyond traditional data-driven benchmark evaluations.

514 6 CONCLUSION

516 We introduced JET EXPANSIONS, a principled framework for restructuring the computational graphs
 517 of large language models. Specialized to LLMs, our method systematically disentangles contribu-
 518 tions of user-selected input→output paths from the overall computation, yielding interpretable
 519 functional components plus a complementary remainder. Operating directly in function space, JET
 520 EXPANSIONS cut through entanglement, respect residual structure, and are grounded in approxima-
 521 tion theory (jets as generalized truncated Taylor operators). This enables modular inspection: one
 522 can pull out paths of interest, e.g., logit lens, n -gram paths, while bracketing the rest as remainder.

524 **Limitations.** JET EXPANSIONS are not strict function approximations in the Taylor sense; they
 525 *rewrite* the computation into interpretable polynomial terms plus a remainder. Remainder size and
 526 alignment with model outputs depend on the jet order k and weight choices (hyperparameters),
 527 and expansions are not unique (higher orders contain lower orders). While graph manipulation
 528 is lightweight, systematic evaluation of many (and higher-order) paths can be costly; heuristics or
 529 subsampling may be needed for large input spaces. Our n -gram studies focused on bi- and tri-grams;
 530 longer-context expansions are left to future work.

531 **Implications and future work.** We envision a Fourier-transform style decomposition for LLMs
 532 and JET EXPANSIONS is perhaps only one way of choosing the basis. Theoretically, we aim to
 533 connect with attribution (e.g., Shapley values), and formalize model equivalence via jet spaces to
 534 ground model diffing. We see fruitful links to linear algebraic decompositions and to Markov/HMM
 535 viewpoints (e.g., structured decoding (Zhang et al., 2023)). We will also study the implications of
 536 the super-exponential path growth with depth. Practically, beyond longer n -grams, we will develop
 537 safety tools (e.g., search features for unwanted associations or PII leakage). Finally, although our
 538 experiments are mainly observational, `jet_expand` may help guide *interventions*, complementing
 539 causal tracing (Meng et al., 2022) and path patching (Goldowsky-Dill et al., 2023).

540
541
ETHICS STATEMENT

542 This work focuses on developing a mathematical framework (JET EXPANSIONS) for analyzing large
 543 language models. Our study does not involve human subjects, proprietary or sensitive data, or ex-
 544 periments that raise privacy, security, or legal concerns. We acknowledge that interpretability tools
 545 may potentially be misused to extract or expose harmful content (e.g., toxic or private knowledge)
 546 embedded in pretrained models. We use the public datasets for LLM toxicity research. We empha-
 547 size that our intent is to promote transparency, safety, and responsible analysis of LLMs, and we
 548 recommend future work carefully consider these implications in line with the ICLR Code of Ethics.
 549

550
551
REPRODUCIBILITY STATEMENT

552 We have taken steps to ensure the reproducibility of our results. All definitions, assumptions, and
 553 theoretical proofs are included in the main text and appendix. Detailed algorithms (Algorithm 1,
 554 Algorithm 2) and mathematical derivations are provided for clarity. Experimental procedures, model
 555 families used (GPT-2, GPT-Neo, LLaMA, OLMo), and metrics are described in Section 5.2 and
 556 Appendix F. We will open-source the code implementing JET EXPANSIONS, extracting jet n -grams,
 557 and reproducing jet lenses, ensuring that all empirical results reported can be replicated.
 558

559
560
LLM USAGE ACKNOWLEDGMENTS

561 We used LLMs to assist with grammar and writing polishing. All equations, analysis, and research
 562 contributions are entirely our own.
 563

564
565
REFERENCES

- 566 Yuntao Bai, Andy Jones, Kamal Ndousse, Amanda Askell, Anna Chen, Nova DasSarma, Dawn
 567 Drain, Stanislav Fort, Deep Ganguli, Tom Henighan, et al. Training a helpful and harmless
 568 assistant with reinforcement learning from human feedback. *arXiv preprint arXiv:2204.05862*,
 569 2022.
- 570 Nora Belrose, Zach Furman, Logan Smith, Danny Halawi, Igor Ostrovsky, Lev McKinney, Stella
 571 Biderman, and Jacob Steinhardt. Eliciting latent predictions from transformers with the tuned
 572 lens. *arXiv preprint arXiv:2303.08112*, 2023.
- 573 Nora Belrose, Quintin Pope, Lucia Quirke, Alex Mallen, and Xiaoli Fern. Neural networks learn
 574 statistics of increasing complexity. *arXiv preprint arXiv:2402.04362*, 2024.
- 575 Jesse Bettencourt, Matthew J. Johnson, and David Duvenaud. Taylor-mode automatic differentiation
 576 for higher-order derivatives in JAX. In *Program Transformations for ML Workshop at NeurIPS*
 577 2019, 2019. URL <https://openreview.net/forum?id=SkxEF3FNPH>.
- 578 Sid Black, Leo Gao, Phil Wang, Connor Leahy, and Stella Biderman. GPT-Neo: Large Scale Autore-
 579 gressive Language Modeling with Mesh-Tensorflow, March 2021. URL <https://doi.org/10.5281/zenodo.5297715>. If you use this software, please cite it using these metadata.
- 580 Tolga Bolukbasi, Adam Pearce, Ann Yuan, Andy Coenen, Emily Reif, Fernanda Viégas, and Martin
 581 Wattenberg. An interpretability illusion for bert. *arXiv preprint arXiv:2104.07143*, 2021.
- 582 James Bradbury, Roy Frostig, Peter Hawkins, Matthew James Johnson, Chris Leary, Dougal
 583 Maclaurin, George Necula, Adam Paszke, Jake VanderPlas, Skye Wanderman-Milne, and Qiao
 584 Zhang. JAX: composable transformations of Python+NumPy programs, 2018. URL <http://github.com/google/jax>.
- 585 Thorsten Brants, Ashok Popat, Peng Xu, Franz Josef Och, and Jeffrey Dean. Large language models
 586 in machine translation. In *Proceedings of the 2007 Joint Conference on Empirical Methods in
 587 Natural Language Processing and Computational Natural Language Learning (EMNLP-CoNLL)*,
 588 pp. 858–867, 2007.

- 594 Trenton Bricken, Adly Templeton, Joshua Batson, Brian Chen, Adam Jermyn, Tom Con-
 595 erly, Nick Turner, Cem Anil, Carson Denison, Amanda Askell, Robert Lasenby, Yifan Wu,
 596 Shauna Kravec, Nicholas Schiefer, Tim Maxwell, Nicholas Joseph, Zac Hatfield-Dodds, Alex
 597 Tamkin, Karina Nguyen, Brayden McLean, Josiah E Burke, Tristan Hume, Shan Carter,
 598 Tom Henighan, and Christopher Olah. Towards monosemanticity: Decomposing language
 599 models with dictionary learning. *Transformer Circuits Thread*, 2023. <https://transformer->
 600 [circuits.pub/2023/monosemantic-features/index.html](https://transformer-circuits.pub/2023/monosemantic-features/index.html).
- 601 Tom Brown, Benjamin Mann, Nick Ryder, Melanie Subbiah, Jared D Kaplan, Prafulla Dhariwal,
 602 Arvind Neelakantan, Pranav Shyam, Girish Sastry, Amanda Askell, et al. Language mod-
 603 els are few-shot learners. *Advances in neural information processing systems*, 33:1877–1901,
 604 2020. URL https://proceedings.neurips.cc/paper_files/paper/2020/file/1457c0d6bfc4967418bfb8ac142f64a-Paper.pdf.
- 605 Nicola Cancedda. Spectral filters, dark signals, and attention sinks, 2024.
- 606 Nicholas Carlini, Florian Tramer, Eric Wallace, Matthew Jagielski, Ariel Herbert-Voss, Katherine
 607 Lee, Adam Roberts, Tom Brown, Dawn Song, Ulfar Erlingsson, et al. Extracting training data
 608 from large language models. In *30th USENIX security symposium (USENIX Security 21)*, pp.
 609 2633–2650, 2021.
- 610 Donnella S Comeau, Danielle S Bitterman, and Leo Anthony Celi. Preventing unrestricted and un-
 611 monitored ai experimentation in healthcare through transparency and accountability. *npj Digital
 612 Medicine*, 8(1):42, 2025.
- 613 Arthur Conmy, Augustine Mavor-Parker, Aengus Lynch, Stefan Heimersheim, and Adrià Garriga-
 614 Alonso. Towards automated circuit discovery for mechanistic interpretability. In A. Oh,
 615 T. Naumann, A. Globerson, K. Saenko, M. Hardt, and S. Levine (eds.), *Advances in Neu-
 616 ral Information Processing Systems*, volume 36, pp. 16318–16352. Curran Associates, Inc.,
 617 2023. URL https://proceedings.neurips.cc/paper_files/paper/2023/file/34e1dbe95d34d7ebaf99b9bcaeb5b2be-Paper-Conference.pdf.
- 618 Charles Ehresmann. Les prolongements d'une variété différentiable: l'espace des jets d'ordre r de
 619 v_n dans v_m . *C. R. Acad. Sci. Paris*, 233:777–779, 1951.
- 620 Maha Elbayad, Jiatao Gu, Edouard Grave, and Michael Auli. Depth-adaptive transformer. *ICLR*,
 621 2020.
- 622 Nelson Elhage, Neel Nanda, Catherine Olsson, Tom Henighan, Nicholas Joseph, Ben Mann,
 623 Amanda Askell, Yuntao Bai, Anna Chen, Tom Conerly, Nova DasSarma, Dawn Drain, Deep
 624 Ganguli, Zac Hatfield-Dodds, Danny Hernandez, Andy Jones, Jackson Kernion, Liane Lovitt,
 625 Kamal Ndousse, Dario Amodei, Tom Brown, Jack Clark, Jared Kaplan, Sam McCandlish, and
 626 Chris Olah. A mathematical framework for transformer circuits. *Transformer Circuits Thread*,
 627 2021. <https://transformer-circuits.pub/2021/framework/index.html>.
- 628 Nelson Elhage, Tristan Hume, Catherine Olsson, Nicholas Schiefer, Tom Henighan, Shauna
 629 Kravec, Zac Hatfield-Dodds, Robert Lasenby, Dawn Drain, Carol Chen, Roger Grosse,
 630 Sam McCandlish, Jared Kaplan, Dario Amodei, Martin Wattenberg, and Christopher Olah.
 631 Toy models of superposition. *Transformer Circuits Thread*, 2022. <https://transformer->
 632 [circuits.pub/2022/toy_model/index.html](https://transformer-circuits.pub/2022/toy_model/index.html).
- 633 Laura Fernández-Becerra, Miguel Ángel González-Santamaría, Ángel Manuel Guerrero-Higueras,
 634 Francisco Javier Rodríguez-Lera, and Vicente Matellán Olivera. Enhancing trust in autonomous
 635 agents: An architecture for accountability and explainability through blockchain and large lan-
 636 guage models. *arXiv preprint arXiv:2403.09567*, 2024.
- 637 Javier Ferrando and Elena Voita. Information flow routes: Automatically interpreting language
 638 models at scale. *arXiv preprint arXiv:2403.00824*, 2024.
- 639 Javier Ferrando, Gabriele Sarti, Arianna Bisazza, and Marta R Costa-jussà. A primer on the inner
 640 workings of transformer-based language models. *arXiv preprint arXiv:2405.00208*, 2024.

- 648 Samuel Gehman, Suchin Gururangan, Maarten Sap, Yejin Choi, and Noah A. Smith. RealToxic-
 649 ityPrompts: Evaluating neural toxic degeneration in language models. In Trevor Cohn, Yulan
 650 He, and Yang Liu (eds.), *Findings of the Association for Computational Linguistics: EMNLP*
 651 2020, pp. 3356–3369, Online, November 2020. Association for Computational Linguistics.
 652 doi: 10.18653/v1/2020.findings-emnlp.301. URL <https://aclanthology.org/2020.findings-emnlp.301>.
- 653
- 654 Mor Geva, Roei Schuster, Jonathan Berant, and Omer Levy. Transformer feed-forward layers
 655 are key-value memories. In Marie-Francine Moens, Xuanjing Huang, Lucia Specia, and Scott
 656 Wen-tau Yih (eds.), *Proceedings of the 2021 Conference on Empirical Methods in Natural Lan-*
 657 *guage Processing*, pp. 5484–5495, Online and Punta Cana, Dominican Republic, November
 658 2021. Association for Computational Linguistics. doi: 10.18653/v1/2021.emnlp-main.446. URL
 659 <https://aclanthology.org/2021.emnlp-main.446>.
- 660
- 661 Mor Geva, Avi Caciularu, Kevin Wang, and Yoav Goldberg. Transformer feed-forward layers build
 662 predictions by promoting concepts in the vocabulary space. In *Proceedings of the 2022 Confer-*
 663 *ence on Empirical Methods in Natural Language Processing*, pp. 30–45, 2022.
- 664 Nicholas Goldowsky-Dill, Chris MacLeod, Lucas Sato, and Aryaman Arora. Localizing model
 665 behavior with path patching. *arXiv preprint arXiv:2304.05969*, 2023.
- 666
- 667 Joshua T Goodman. A bit of progress in language modeling. *Computer Speech & Language*, 15(4):
 668 403–434, 2001.
- 669
- 670 Andreas Griewank and Andrea Walther. *Evaluating derivatives: principles and techniques of algo-*
 671 *rithmic differentiation*. SIAM, 2008.
- 672
- 673 Dirk Groeneveld, Iz Beltagy, Pete Walsh, Akshita Bhagia, Rodney Kinney, Oyvind Tafjord,
 674 Ananya Harsh Jha, Hamish Ivison, Ian Magnusson, Yizhong Wang, et al. Olmo: Accelerating the
 675 science of language models. *arXiv preprint arXiv:2402.00838*, 2024.
- 676
- 677 Thomas Hartvigsen, Saadia Gabriel, Hamid Palangi, Maarten Sap, Dipankar Ray, and Ece Ka-
 678 mar. ToxiGen: A large-scale machine-generated dataset for adversarial and implicit hate speech
 679 detection. In Smaranda Muresan, Preslav Nakov, and Aline Villavicencio (eds.), *Proceedings*
 680 *of the 60th Annual Meeting of the Association for Computational Linguistics (Volume 1: Long*
 681 *Papers)*, pp. 3309–3326, Dublin, Ireland, May 2022. Association for Computational Linguis-
 682 *tics*. doi: 10.18653/v1/2022.acl-long.234. URL <https://aclanthology.org/2022.acl-long.234>.
- 683
- 684 Kai He, Rui Mao, Qika Lin, Yucheng Ruan, Xiang Lan, Mengling Feng, and Erik Cambria. A survey
 685 of large language models for healthcare: from data, technology, and applications to accountability
 686 and ethics. *Information Fusion*, 118:102963, 2025.
- 687
- 688 Kaiming He, Xiangyu Zhang, Shaoqing Ren, and Jian Sun. Deep residual learning for image recog-
 689 *nition*. In *Proceedings of the IEEE conference on computer vision and pattern recognition*, pp.
 690 770–778, 2016.
- 691
- 692 Stanislaw Jastrzebski, Devansh Arpit, Nicolas Ballas, Vikas Verma, Tong Che, and Yoshua Bengio.
 693 Residual connections encourage iterative inference. *arXiv preprint arXiv:1710.04773*, 2017.
- 694
- 695 Jiacheng Liu, Sewon Min, Luke Zettlemoyer, Yejin Choi, and Hannaneh Hajishirzi. Infini-
 696 gram: Scaling unbounded n-gram language models to a trillion tokens. *arXiv preprint*
 697 *arXiv:2401.17377*, 2024.
- 698
- 699 Kevin Meng, David Bau, Alex Andonian, and Yonatan Belinkov. Locating and editing factual
 700 associations in gpt. *Advances in Neural Information Processing Systems*, 35:17359–17372, 2022.
- 701
- 702 Jack Merullo, Carsten Eickhoff, and Ellie Pavlick. Language models implement simple word2vec-
 703 style vector arithmetic. *arXiv e-prints*, pp. arXiv–2305, 2023.
- 704
- 705 Eric Mitchell, Charles Lin, Antoine Bosselut, Chelsea Finn, and Christopher D Manning. Fast model
 706 editing at scale. In *International Conference on Learning Representations*, 2021.

- 702 Eric Mitchell, Charles Lin, Antoine Bosselut, Christopher D Manning, and Chelsea Finn. Memory-
 703 based model editing at scale. In *International Conference on Machine Learning*, pp. 15817–
 704 15831. PMLR, 2022.
- 705 Aaron Mueller. Missed causes and ambiguous effects: Counterfactuals pose challenges for inter-
 706 preting neural networks. *arXiv preprint arXiv:2407.04690*, 2024.
- 707 Timothy Nguyen. Understanding transformers via n-gram statistics. *arXiv preprint*
 708 *arXiv:2407.12034*, 2024.
- 709 nostalgebraist. logit lens on non-gpt2 models + extensions, 2021a. URL <https://colab.research.google.com/drive/1MjdfK2srcerLrAJDRaJQK00sUiZ-hQtA>.
- 710 nostalgebraist. interpreting gpt: the logit lens, 2021b. URL <https://www.lesswrong.com/posts/AcKRB8wDpdaN6v6ru/interpreting-gpt-the-logit-lens#HEf5abD7hqqAY2GSQ>.
- 711 Priyadarshini Panda, Abhroni Sengupta, and Kaushik Roy. Conditional deep learning for energy-
 712 efficient and enhanced pattern recognition. In *2016 Design, Automation & Test in Europe Con-
 713 ference & Exhibition (DATE)*, pp. 475–480, 2016.
- 714 Alethea Power, Yuri Burda, Harri Edwards, Igor Babuschkin, and Vedant Misra. Grokking: Gen-
 715 eralization beyond overfitting on small algorithmic datasets, 2022.
- 716 Alec Radford, Jeff Wu, Rewon Child, David Luan, Dario Amodei, and Ilya Sutskever. Language
 717 models are unsupervised multitask learners. 2019.
- 718 Emmanuel K Raptis, Athanasios Ch Kapoutsis, and Elias B Kosmatopoulos. Agentic llm-based
 719 robotic systems for real-world applications: a review on their agenticness and ethics. *Frontiers in
 720 Robotics and AI*, 12:1605405, 2025.
- 721 Baptiste Rozière, Jonas Gehring, Fabian Gloeckle, Sten Sootla, Itai Gat, Xiaoqing Ellen Tan, Yossi
 722 Adi, Jingyu Liu, Romain Sauvestre, Tal Remez, Jérémie Rapin, Artyom Kozhevnikov, Ivan Ev-
 723 timov, Joanna Bitton, Manish Bhatt, Cristian Canton Ferrer, Aaron Grattafiori, Wenhan Xiong,
 724 Alexandre Défossez, Jade Copet, Faisal Azhar, Hugo Touvron, Louis Martin, Nicolas Usunier,
 725 Thomas Scialom, and Gabriel Synnaeve. Code llama: Open foundation models for code, 2024.
- 726 Harshay Shah, Andrew Ilyas, and Aleksander Madry. Decomposing and editing predictions by
 727 modeling model computation. *arXiv preprint arXiv:2404.11534*, 2024.
- 728 Claude Elwood Shannon. A mathematical theory of communication. *The Bell system technical
 729 journal*, 27(3):379–423, 1948.
- 730 Helena Smith. Clinical ai: opacity, accountability, responsibility and liability. *AI & Society*, 36:
 731 535–545, 2021. doi: 10.1007/s00146-020-01019-6.
- 732 Luca Soldaini, Rodney Kinney, Akshita Bhagia, Dustin Schwenk, David Atkinson, Russell Author,
 733 Ben Bogin, Khyathi Chandu, Jennifer Dumas, Yanai Elazar, Valentin Hofmann, Ananya Harsh
 734 Jha, Sachin Kumar, Li Lucy, Xinxi Lyu, Nathan Lambert, Ian Magnusson, Jacob Morrison, Niklas
 735 Muennighoff, Aakanksha Naik, Crystal Nam, Matthew E. Peters, Abhilasha Ravichander, Kyle
 736 Richardson, Zejiang Shen, Emma Strubell, Nishant Subramani, Oyvind Tafjord, Pete Walsh, Luke
 737 Zettlemoyer, Noah A. Smith, Hannaneh Hajishirzi, Iz Beltagy, Dirk Groeneveld, Jesse Dodge,
 738 and Kyle Lo. Dolma: An Open Corpus of Three Trillion Tokens for Language Model Pretraining
 739 Research. *arXiv preprint*, 2024. URL <https://arxiv.org/abs/2402.00159>.
- 740 Anej Sveti and Ryan Cotterell. Transformers can represent n-gram language models. *arXiv preprint*
 741 *arXiv:2404.14994*, 2024.
- 742 Adly Templeton, Tom Conerly, Jonathan Marcus, Jack Lindsey, Trenton Bricken, Brian Chen,
 743 Adam Pearce, Craig Citro, Emmanuel Ameisen, Andy Jones, Hoagy Cunningham, Nicholas L
 744 Turner, Callum McDougall, Monte MacDiarmid, C. Daniel Freeman, Theodore R. Sumers,
 745 Edward Rees, Joshua Batson, Adam Jermyn, Shan Carter, Chris Olah, and Tom Henighan.
 746 Scaling monosemanticity: Extracting interpretable features from claude 3 sonnet. *Trans-
 747 former Circuits Thread*, 2024. URL <https://transformer-circuits.pub/2024/scaling-monosemanticity/index.html>.

- 756 Hugo Touvron, Thibaut Lavril, Gautier Izacard, Xavier Martinet, Marie-Anne Lachaux, Timothée
 757 Lacroix, Baptiste Rozière, Naman Goyal, Eric Hambro, Faisal Azhar, et al. Llama: Open and
 758 efficient foundation language models. *arXiv preprint arXiv:2302.13971*, 2023a.
- 759
- 760 Hugo Touvron, Louis Martin, Kevin Stone, Peter Albert, Amjad Almahairi, Yasmine Babaei, Niko-
 761 lay Bashlykov, Soumya Batra, Prajjwal Bhargava, Shruti Bhosale, et al. Llama 2: Open founda-
 762 tion and fine-tuned chat models. *arXiv preprint arXiv:2307.09288*, 2023b.
- 763
- 764 Ashish Vaswani, Noam Shazeer, Niki Parmar, Jakob Uszkoreit, Llion Jones, Aidan N Gomez,
 765 Łukasz Kaiser, and Illia Polosukhin. Attention is all you need. *Advances in neural informa-*

766 *767*
 768 Andreas Veit, Michael J Wilber, and Serge Belongie. Residual networks behave like ensembles of
 relatively shallow networks. *Advances in neural information processing systems*, 29, 2016.

769

770 Elena Voita, Javier Ferrando, and Christoforos Nalmpantis. Neurons in large language models:
 771 Dead, n-gram, positional. In Lun-Wei Ku, Andre Martins, and Vivek Srikumar (eds.), *Findings*
 772 *773*
 774 of the Association for Computational Linguistics ACL 2024, pp. 1288–1301, Bangkok, Thailand
 775 and virtual meeting, August 2024. Association for Computational Linguistics. URL <https://aclanthology.org/2024.findings-acl.75>.

776

777 Sandra Wachter, Brent Mittelstadt, and Luciano Floridi. Transparent, explainable, and accountable
 778 ai for robotics. *Science robotics*, 2(6):eaan6080, 2017.

779

780 Kevin Wang, Alexandre Variengien, Arthur Conmy, Buck Shlegeris, and Jacob Steinhardt. Inter-
 781 pretability in the wild: a circuit for indirect object identification in gpt-2 small. *arXiv preprint*
 782 *783*
 784 *785*
 785 arXiv:2211.00593, 2022.

786

787 Xiangxiang Xu, Shao-Lun Huang, Lizhong Zheng, and Gregory W Wornell. An information theo-
 788 retic interpretation to deep neural networks. *Entropy*, 24(1):135, 2022.

789

790

791

792

793

794

795

796

797

798

799

800

801

802

803

804

805

806

807

808

809

810 **A JETS AND EXPANSIONS**
 811

812 A jet of a function represents an equivalence class. We thus can perform algebraic operations among
 813 functional equivalence classes using jet algebra stated below.

814 **Proposition 1** (Jet algebra). *Let $f, g \in C^\infty(\mathbb{R}^d, \mathbb{R}^d)$ and $k \in \mathbb{N}^+$. Then,*

- 815 *(i) $J^k(af + bg)(\mathbf{x}_0) = a J^k(f)(\mathbf{x}_0) + b J^k(g)(\mathbf{x}_0)$, for $a, b \in \mathbb{R}$ (linearity);*
 816 *(ii) $J^k f(\mathbf{x}_0) \circ g \in J^k f(\mathbf{x}_0)$ and $J^k f(\mathbf{x}_0) \circ g(y) = J^k f(\mathbf{x}_0)(g(y))$ (jet after endomorphisms);*
 817 *(iii) $g \circ J^k f(\mathbf{x}_0) = \{g \circ u : u \in J^k f(x)\}$ (endomorphism after jet);*
 818 *(iv) $J^k(f \circ g)(\mathbf{x}_0) = J^k f(g(\mathbf{x})) \circ J^k g(\mathbf{x}_0)$ (composition of jets);*

819 Properties (i)-(iii) follow directly from the definition; (iv) is a consequence of the chain rule and truncation.
 820 To reorganize residual computations typically used in LLMs, we rely on the disentangling
 821 property of jets, restated below.

822 **Lemma 1** (Disentanglement of Jets). *Let $f \in C^\infty(\mathbb{R}^d, \mathbb{R}^d)$, $k \in \mathbb{N}$, $N \in \mathbb{N}^+$, $\{\mathbf{x}_i\}_{i=1}^N$ be a set of
 823 jet base points, and $w \in \Delta^{N-1} \subset \mathbb{R}^N$ be a set of jet weights (i.e., $w_i \geq 0$, $\sum_i w_i = 1$). Define the
 824 sum $\bar{x} = \sum_{i=1}^N x_i$ and $r = \max_i w_i \|x_i - \bar{x}\|$. Then the k -jet of f at the sum \bar{x} satisfies*

825
$$J^k f \left(\sum_{i=1}^N \mathbf{x}_i \right) = \sum_{i=1}^N w_i J^k f(\mathbf{x}_i) + O(r^{k+1}).$$

826 **Proof of Lemma 1** Take $y \in \mathbb{R}^d$, $N \geq 1$, the set of jet base points $x_i \in \mathbb{R}^d$ for $i \in [N]$, jet weights
 827 $w \in \Delta^{N-1}$ and an order $k \geq 0$. Since w belongs to the simplex Δ^{N-1} , we have $\sum_{i=1}^N w_i = 1$.
 828 Multiplying $f(y)$ on both hands, we obtain

829
$$\sum_{i=1}^N w_i f(y) = f(y).$$

830 Applying eq. (3) (Taylor expansion) and the definition of jet with each x_i as the center, the left hand
 831 side (LHS) becomes

832
$$\sum_{i=1}^N w_i f(y) = \sum_{i=1}^N w_i \left[f(x_i) + \sum_{s=1}^k D^s f(x_i)(y - x_i)^{\otimes s} + O(\|y - x_i\|^{k+1}) \right] \quad (7)$$

833
$$= \sum_{i=1}^N w_i J^k f(\mathbf{x}_i)(y) + O(w_i \|y - x_i\|^{k+1}), \quad (8)$$

834 At the same time, we can expand $f(y)$ at the right hand side (RHS) with $\sum_{i=1}^N x_i$ as the center

835
$$f(y) = J^k f \left(\sum_{i=1}^N \mathbf{x}_i \right)(y) + O(\|y - \sum_{i=1}^N x_i\|^{k+1}).$$

836 Now let us take $y = \sum_{i=1}^N x_i$ and observe that the remainder at RHS vanishes $O(\|y - \sum_{i=1}^N x_i\|^{k+1}) = 0$ and the remainder at LHS $O(w_i \|y - x_i\|^{k+1}) = O(w_i \|x_i - \sum_j x_j\|^{k+1})$. Finally we observe
 837 that the class of functions in the last O are dominated by the class of function in $O(r^{k+1})$ where
 838 $r = \max_i \{w_i \|x_i - \sum_j x_j\|\}$ is the maximum remainder. This concludes the proof.

839 As a side note, jet weights would not need to form convex combinations, but rather linear combinations $\sum_i w_i = 1$. However, restricting to convex combinations has two major advantages:

- 840
 - 841 optimizing over a convex set guarantees the existence of maxima and minima (Weierstrass
 842 theorem) and uniqueness of minima if we are optimizing a strictly convex loss as in general
 843 is the case for expansions that only affect the decoder module.
 - 844 weights within the probability simplex have a clearer interpretation for interpretability pur-
 845 poses.

864 **B REMAINDER SIZE OF JET EXPANSIONS**
865866 JET EXPANSIONS does not aim to provide approximation guarantees. Instead, in the following we
867 clarify when small remainders are expected (input-specific cases) and when they are not (function-
868 level expansions), but the expansions still yield meaningful, interpretable insights.
869870 In *input-specific* evaluations (where we choose specific input sentences like “new simple neural
871 architecture, the Transformer”), we expect reminders to be small, since we want to draw specific
872 conclusions about how a model is behaving on a particular input. In these cases (i.e. in the Jet
873 lenses experiments of §5.2.1) we do provide empirical studies, and we often find that the remainder
874 δ is small. In order to measure the remainder between the expansion logit and the model logit,
875 we compute the cosine similarity between them, since direct difference depends heavily on the input
876 sentences (See App. F, “Cosine similarity as a remainder metric.”). In short, we use cosine similarity
877 as an indicator for checking if the remainder is small. Most of our heatmaps in the submission
878 include this similarity measures in the parenthesis e.g. “Expan. (0.993)”. We also compute average
879 similarities over 100 examples and summarize the results in Figure 4 (bottom): expansion logits
880 are frequently close to the model outputs, with cosine similarities in the 0.85–1 range, indicating
881 that the extracted components capture most of the behavior for many concrete inputs i.e. smaller
882 remainders. In general, the remainder size will depend on three factors:
883

- 884
1. the type of jet expansion one performs (e.g. iterative vs joint);
885
 2. the non-linearity on which the jet is applied to (e.g. ReLu vs ELu, vs LayerNorm)
886
 3. how far the variate is from the base point, which in turn fully depends on the chosen input
sentence (see Equation (4)).

887 In *function-level* expansions (e.g., around the embedding function Enc for extracting jet bi-grams),
888 remainders can be large and this is fully expected. Here, the goal is not approximation accuracy but
889 to decompose the computation into interpretable paths. Concretely, let us consider bi-grams (§5.2.2):
890 the model performs far more than the isolated mechanism of predicting a token based solely on the
891 previous one. Therefore we do expect reminders between the model output and the extracted bi-
892 gram paths to be *naturally* large. Yet the extracted paths remain *meaningful* precisely because they
893 isolate a coherent part of the computation, even if they explain only a small fraction of the total
894 behavior. A large remainder therefore does not invalidate the interpretation; it simply reflects that
895 we are focusing on one specific, coherent part of the computation. This is a common situation
896 across interpretability research, or in general when humans try to explain things. Conceptually,
897 we find it useful to compare jet expansions to Fourier transform: even when the Fourier transform
898 captures only part of the signal’s spectrum and the resulting approximation error cannot be directly
899 measured, the partial frequency information it provides can still be valuable for understanding the
900 signal and diagnosing issues in the generating circuits.
901902 **C EXPONENTIAL EXPANSION AND ENSEMBLING PERSPECTIVE ON LLM
903 COMPUTATION**904 Algorithm 2 recursively expands at all residual blocks. We see it as the maximal expansion (the
905 upper limit of expansion) of JET EXPANSIONS. It aims to demonstrate that JET EXPANSIONS also
906 provides theoretical grounds for Veit et al. (2016), whose analysis at the time lacked theoretical
907 foundations and was presented heuristically and empirically, by manually selecting paths (i.e., 2^L
908 gradient paths) for analyzing model behavior, where the exponentially many ensemble structures
909 were syntactically noted rather than analytically derived.
910911 With a closer look, we were surprised to find that several empirical procedures used in Veit et al.
912 (2016) are exactly recoverable as specific instances of jet expansions. For example, the deletion of
913 a module (Sec. 4.1 in Veit et al. (2016)) corresponds precisely to

914
$$\text{jet_expand}(f, l, h_{l-2}, 0),$$

915 i.e., a JET EXPANSIONS with the skip-layer upstream stream as the base point and with jet order 0.
916917 Another example is their gradient analysis. In the original exposition, the procedure is described
918 operationally as: “*To sample a path of length k , we first feed a batch forward through the whole*

network. During the backward pass, we randomly sample k residual blocks. For those k blocks, we only propagate through the residual module; for the remaining $n - k$ blocks, we only propagate through the skip connection.” The outcome of these operational steps is equal to taking the derivative component of a first-order jet expansion over each block and evaluate it over a batch of inputs, as shown below. Note that the following reinterpretation focus on the gradients with respect to intermediate representations while empirically collecting gradients with respect to parameters is much easier.

Path selection in backpropagation as first-order JET EXPANSIONS. For a residual block,

$$\beta_l(h_{l-1}) = (\text{id} + \gamma_l) \circ h_{l-1} = h_{l-1} + \gamma_l(h_{l-1}),$$

the derivative satisfies $D\beta_l[h_{l-1}] = I + D\gamma_l[h_{l-1}]$. Thus, propagating gradients through the full network $f = \beta_L \circ \beta_{L-1} \circ \dots \circ \beta_1$ yields the Jacobian using the chain rule

$$Df(x_0) = \prod_{l=1}^L (I + D\gamma_l[x_{h-1}]).$$

On the other hand, the first-order jet of a residual block at h_{l-1} is

$$J^1(\beta_l)(h_{l-1}) = (\beta_l(h_{l-1}), I + D\gamma_l[h_{l-1}]),$$

where we use the pair notation for the jet, the first entry being the zero-th order term and the second entry being the first order term. Since jets compose according to

$$J^1(f \circ g)(x) = J^1 f(g(x)) \circ J^1 g(x) \quad (\text{Proposition 1(iv)}),$$

we have the full first-order jet of f as

$$J^1(f)(x_0) = J^1(\beta_L)(h_{L-1}) \circ \dots \circ J^1(\beta_1)(x_0),$$

Extracting the derivative component of this composite jet therefore yields the ordered product of the derivative factors from each block:

$$Df(x_0) = (I + D\gamma_L[h_{L-1}]) \circ (I + D\gamma_{L-1}[h_{L-2}]) \circ \dots \circ (I + D\gamma_1[x_0]).$$

Composition of first-order jets multiplies the linear parts in this precise order:

$$Df(x_0) = (I + D\gamma_L[h_{L-1}]) \dots (I + D\gamma_1[x_0]).$$

Expanding this product produces 2^L additive terms:

$$Df(x_0) = \sum_{S \subseteq \{1, \dots, L\}} \left(\prod_{l \in S} D\gamma_l[h_{l-1}] \right),$$

each corresponding to a distinct choice of either I or $D\gamma_l$ at every block. These terms match exactly, one-for-one, the “gradient paths” enumerated by Veit et al. (2016). Their operational procedure (“selecting” residual or skip gradients per block) amounts to selecting individual terms from this expansion. Consequently, their “gradient paths” are not independent computational input-output paths through the nonlinear network, but the combinatorial derivative components of the first-order jet (i.e., the first order term) of the residual network.

D RUNTIME OF JET EXPANSIONS

We report in fig. 5 a plot of the runtime for evaluating expansions originating from the joint jet lenses of section 5.2.1 as a ratio of the input model evaluation (forward pass), for both the uniform and the optimized jet weights w setup, for different jet orders k .

E JET n -GRAMS AND THEIR ALGORITHMS

General concept of n -gram models The general concept of n -gram models linked to (transformer-based) language models involves defining or constructing mappings that functionally depend only on $n - 1$ input tokens (with the n -th token being the output token) to capture and describe the behaviour of the original language models. We are not the first to explore this idea; for instance Nguyen (2024) fits n -grams on the same dataset used to train the language models.

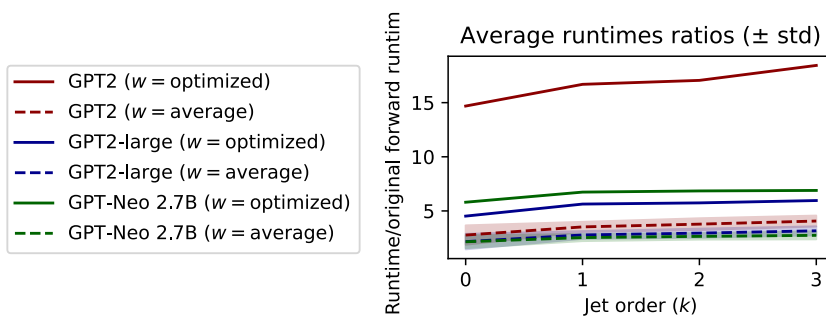


Figure 5: Empirical runtime of evaluations of JET EXPANSIONS originating from the joint jet lenses as a ratio of the evaluation of the input model.

JET EXPANSIONS for in-model n -grams JET EXPANSIONS allow us to define n -grams statistics that are derived solely and directly from the model itself – producing *in-model* n -grams rather than *in-data* n -grams. This approach offers at least two significant advantages:

- **No repeated inference runs over prepared datasets:** It removes the need to prepare datasets for prompting LLMs, thereby avoiding repeated inference runs to collect activation patterns for interpretability analysis and reducing computational overhead. With a small n , direct expansion of LLMs into n -grams can be performed on CPUs, which are roughly an order of magnitude less expensive than GPUs.
- **Avoidance of fitting artifacts:** It avoids potential artifacts that could arise from the selection of external n -gram fitting methods.

We describe the detailed relationship between JET EXPANSIONS and bi-grams/tri-grams, which we used in our case studies. We will release code for these procedures and also provide equivalent algorithms that directly use transformer modules.

Jet bi-grams Jet bi-grams are paths that do not pass through self-attention layers. In experiments, we focus on two types of bi-gram paths. a) the embedding-unembedding path that can be obtained as $\text{jet_expand}(f, L, \{\text{Enc}\}, 0)$. b) paths that pass through one MLP module, assuming MLPs are at odd block indices in the residual network architecture, the procedure to extract the path is [described from line 3 to line 7 in Algorithm 3](#). This procedure results in a series of functions in ξ , one for each MLP layer, that depend only on the last input token. Applying softmax normalization to their logit output allows these functions to define (conditional) bi-grams.

Jet tri-grams Jet tri-grams involve paths that pass through at least one self-attention layer, with a need to isolate the contribution from the first token of the tri-gram. The procedure for extracting a 0-th order jet trigram path that passes through the i th self-attention layer (assuming it has one head) is [described from line 1 to line 5 in Algorithm 4](#). This procedure yields a map that depends only on two input tokens, isolating the contribution of the i th self-attention layer on pairs of tokens. Once softmax normalization is applied, this defines a tri-gram. The tri-gram could represent either a skip trigram or a contiguous trigram, depending on how positional information is encoded (e.g., absolute positional embeddings versus rotary embeddings).

1026 **Algorithm 3** Dataset-free extraction of jet bi-grams (MLP paths).

1027 **Require:** Model f , total blocks L , vocabulary V
1028
1029 1: // Initialize with encoder path
1030 2: $\mathcal{C} \leftarrow \{\text{Enc}\}$
1031
1032 3: // Iterate over MLP blocks (odd indices)
1033 4: **for** $l = 1, 3, \dots, L$ **do**
1034 5: $(\xi_l, \delta_l) \leftarrow \text{jet_expand}(f, l, \{\text{Enc}\}, 0)$
1035
1036 6: // Collect each expanded MLP term
1037 7: $\mathcal{C} \leftarrow \mathcal{C} \cup \{e(\cdot, 1) \mid e \in \xi_l, e \neq \text{Enc}\}$
1038
1039 8: // Expand over the decoder
1040 9: $(\xi, \delta) \leftarrow \text{jet_expand}(f, L + 1, \mathcal{C}, 0)$
1041
1042 10: // Evaluate over the input space
1043 11: **for all** $e \in \xi$ **do**
1044 12: **for all** $x \in V$ **do**
1045 13: **for all** $i \in V$ **do**
1046 14: Record $(x, i, e(x)[i])$ as the bi-gram score
1047 15: **return** Symbolic bi-gram table $\{(x, i, e(x)[i])\}$

1049 **Algorithm 4** Dataset-free extraction of jet tri-grams (Attention paths).

1050 **Require:** Model f , total blocks L , target self-attention block index l , vocabulary V
1051 1: $\mathcal{C} \leftarrow \{\text{Enc} \circ (x_{t-1}, x_t)\}$
1052
1053 2: // Expand over the attention
1054 3: $(\xi, \delta) \leftarrow \text{jet_expand}(f, l, \mathcal{C}, 0)$
1055 4: $\mathcal{C} \leftarrow \{e(\cdot, 1) \mid e \in \xi_l, e \neq \text{Enc}\}$
1056
1057
1058 5: // Expand over the decoder
1059 6: $(\xi, \delta) \leftarrow \text{jet_expand}(f, L + 1, \mathcal{C}, 0)$
1060
1061 7: // Evaluate over the input space
1062 8: **for all** $e \in \xi$ **do**
1063 9: **for all** $(x_{t-1}, x_t) \in V^2$ **do**
1064 10: **for all** $i \in V$ **do**
1065 11: Record $(x_{t-1}, x_t, i, e(x_{t-1}, x_t)[i])$ as the tri-gram score
1066 12: **return** Symbolic tri-gram table $\{(x_{t-1}, x_t, i, e(x_{t-1}, x_t)[i])\}$

1067
1068
1069
1070
1071
1072
1073
1074
1075
1076
1077
1078
1079

Practical computation vs. formal jet n -grams. Algorithms 3 and 4 express bi-gram and tri-gram extraction in the jet-expansion formalism: we expand intermediate paths using `jet_expand`, collect the resulting functions into \mathcal{C} , and finally obtain a family of zeroth-order jet paths

$$e \in \xi, \quad e : V^{n-1} \rightarrow \mathbb{R}^V,$$

where the arity of e (one token for MLP paths, two tokens for single-attention paths) determines whether the path represents a bi-gram ($n = 2$) or a tri-gram ($n = 3$). Formally, an n -gram table is obtained by exhaustive evaluation of e on its domain: recording $e(x)[i]$ for $x \in V$ in the bi-gram case, or $e(x_{t-1}, x_t)[i]$ for $(x_{t-1}, x_t) \in V^2$ in the tri-gram case. In practical implementations, these evaluations correspond to batched matrix computations over the entire vocabulary. For bi-grams, the embedding matrix $E \in \mathbb{R}^{|V| \times d}$ serves as the batch of all input tokens, and each MLP component represented in \mathcal{C} acts on E via matrix multiplications; after layer normalization and

1080 projection through the unembedding matrix U , the resulting matrix has (x, i) entry equal to $e(x)[i]$.
 1081 For tri-grams, an analogous “pairwise embedding” tensor encodes all (x_{t-1}, x_t) pairs at once, and
 1082 the attention and subsequent linear operators act on this tensor in batch; projection through U yields
 1083 a three-dimensional array whose (x_{t-1}, x_t, i) entry is exactly $e(x_{t-1}, x_t)[i]$. Thus, the formal jet
 1084 description and the practical batched-matrix implementation are two views of the same operation: a
 1085 jet path defines the atomic paths $\{e, e \in \xi\}$ which simplifies the large model, and the bi-gram table
 1086 is obtained by evaluating e simultaneously on all vocabulary elements using matrix multiplications.
 1087

1088 F EXPERIMENTAL METRICS

1090 In this section, we detail the measured quantities in each empirical case study.

1092 **Cosine similarity as a remainder metric.** In Section 5.2.1 (the lens experiments), we need a
 1093 comparable metric for quantifying the size of the remainder term δ in the JET EXPANSIONS for a
 1094 given input sentence. Let $m \in \mathbb{R}^V$ denote the model output logits over the vocabulary V , produced
 1095 by a full forward pass, and let $e \in \mathbb{R}^V$ denote the logits predicted by the truncated jet expansion. A
 1096 naïve approach would define the remainder as the difference vector $r = m - e$ and measure its mag-
 1097 nitude using $\|r\|$. However, this direct norm-based measurement is highly sensitive to input-specific
 1098 variation, such as sequence length, and the internal activation scaling of the model. As a result, the
 1099 magnitude $\|m - e\|$ can be dominated by variations in logit norm rather than reflecting the intrinsic
 1100 approximation error introduced by JET EXPANSIONS. To address this, we adopt cosine similarity
 1101 as a scale-invariant measure of alignment between the model logits and their JET EXPANSIONS
 1102 approximation. Formally, we compute

$$1102 \cos(e, m) = \frac{e \cdot m}{\|e\| \|m\|},$$

1104 where \cdot denotes the standard dot product. A cosine similarity of 1 means that JET EXPANSIONS
 1105 preserves the model logits structurally. Conversely, lower cosine similarity values correspond to a
 1106 larger remainder term in the expansion. Practically, cosine similarity enables us to disentangle re-
 1107 mainder size from input-dependent logit scaling, offering a more interpretable and stable measure of
 1108 the fidelity of JET EXPANSIONS. We therefore report cosine similarity throughout our experiments
 1109 as our primary metric for assessing remainder size.

1110 **Δ Logit after intervention.** In Section 5.2.1, to compute Δ logits, we calculate the logits for the
 1111 given n -gram both before and after applying the intervention, then determine the change in the logits.
 1112 For example, consider the trigram (Lemma, let, s). We compute the logit of “s” conditioned on the
 1113 input “Lemma let”. The intervention involves removing the corresponding attention head (e.g., head
 1114 2). We then measure and report the change in the logit for “s” as a result of this intervention.

1116 **Jet bi-gram comparison for code fine-tuning.** In Section 5.2.2, we derive the top 1000 bigrams
 1117 using Algorithm 3. These bigrams are then saved, for example, as CSV files, enabling the inspec-
 1118 tion and comparison of models via their respective bi-grams. This approach allows us to bypass
 1119 the challenges of comparing models in the high-dimensional parameter space, where measuring
 1120 behavioral-level differences can be difficult. We have developed a web UI demonstration where
 1121 users can perform “model diffs” using the respective jet bi-grams. For example, Figure 6 demon-
 1122 strates how this UI can be used to compare the base Llama-2-7B model with its coding fine-tuned
 1123 versions.

1124 **Jet bi-gram toxic mass.** In Section 5.2.2, we introduce a method to quantify the possession of
 1125 toxic knowledge. We compute jet bigram probability scores and calculate the cumulative conditional
 1126 probability mass over a curated set of toxic bigrams, pairs of tokens specifically linked to toxic
 1127 meanings in a predefined word list. The toxic mass (M) is formally defined as the sum of these
 1128 conditional probabilities across the query set (Q):

$$1130 M = \sum_{z \in Q} P(z_2 | z_1)$$

1131 Here, Q represents the query set comprising the toxic bigrams derived from the word list. In this
 1132 way, we can measure model toxicity using simple query words instead of relying on extensive,
 1133 curated prompting datasets.

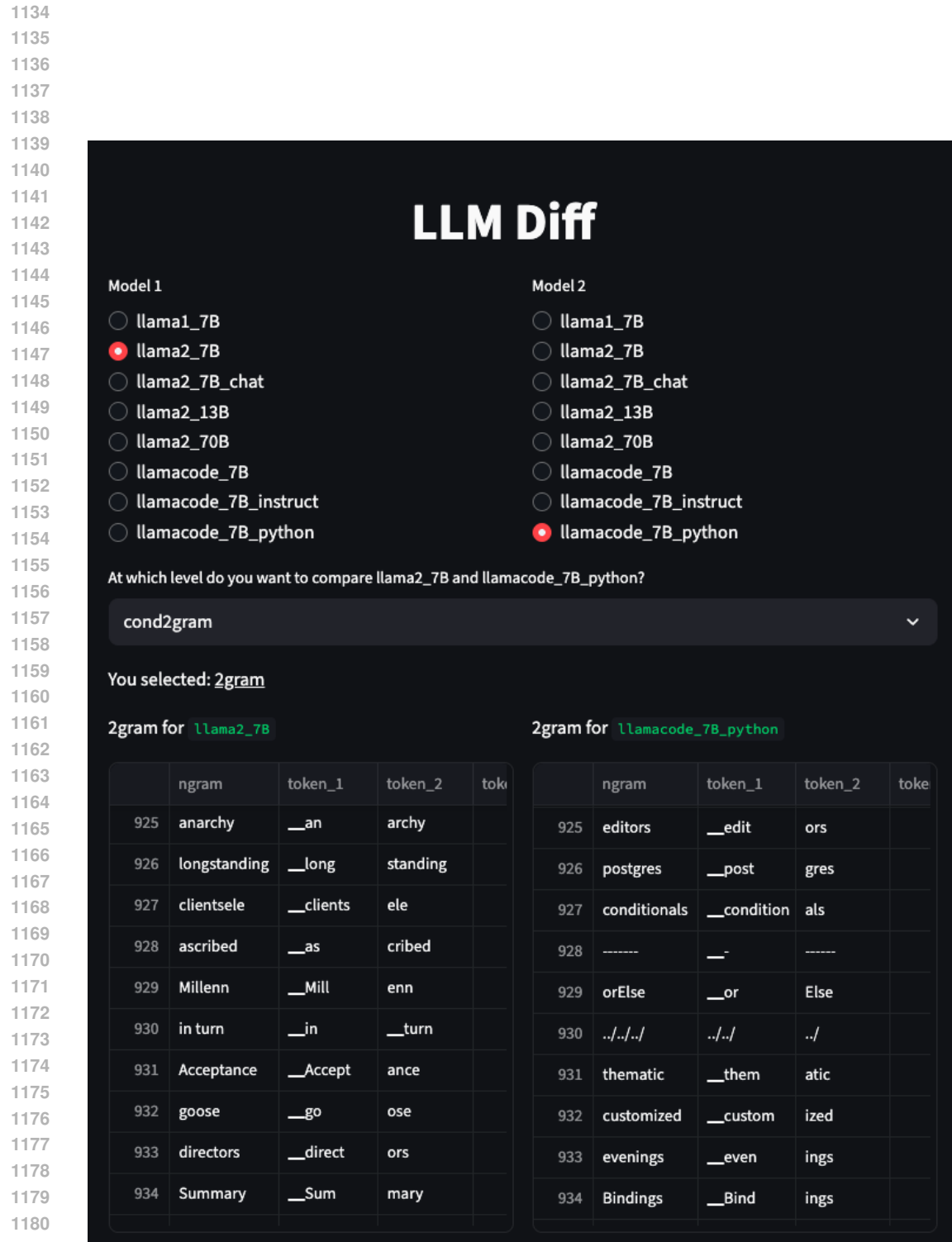


Figure 6: A web UI for running LLM Diff with jet n-grams.

1182
 1183
 1184
 1185
 1186
 1187

1188
 1189 **One-to-one bi-grams like and many-to-many bi-grams.** In Section H, we analyze the pretrain-
 1190 ing dynamics by checking the learning speed of bi-grams from different categories. One-to-one
 1191 bi-grams are (approximately) unimodal bi-grams that concentrate all mass on a single token: i.e.
 1192 given z_1 , $\mathbb{P}_{\mathcal{D}}(z_2|z_1) \approx 1$ and given z_2 , $\mathbb{P}_{\mathcal{D}}(z_1|z_2) \approx 1$ for a specific pair of token and close to 0 for
 1193 all others. In the example in the paper, z_1 = “&”, and z_2 = “amp”. $\mathbb{P}_{\mathcal{D}}$ is the probability distribution
 1194 induced by the pre-training data. Many-to-many bi-grams we refer to the opposite scenario where
 1195 both the conditional probabilities are highly multi-modal. In the example z_1 = “make” and z_2 =
 1196 “sure” we have that many other tokens can succeed z_1 = “make” or precede z_2 = “sure”.
 1197

1198 **Hit ratios of bi-grams.** The Hit Ratio (HR@n), often referred to as hit rate, is a metric commonly
 1199 used in ranking tasks. In our context of Section H, we treat each checkpoint of the language model
 1200 as a “ranker” of bi-grams. The Hit Ratio measures how effectively the current model checkpoint re-
 1201 trieves high-quality bi-grams from the set of all possible bi-grams. To quantify the model’s progress,
 1202 we define the bi-grams at the final step as the “good” bi-grams and measure how quickly the model
 1203 approaches these high-quality bi-grams. Specifically, we compute the HR@n to evaluate how often
 1204 the model’s output bi-grams match those in the “true” top n ranked bi-grams given by the final step.
 1205 Formally, the Hit Ratio@n is given by

$$1205 \quad \text{HR@n} = \frac{1}{n} \sum_{i=1}^n \mathbb{I}(\text{the } i\text{-th bi-gram output by the current model} \in \text{True_Top_n})$$

1206 where n is the number of top predictions being considered and

- 1207
- 1208 • \mathbb{I} is the indicator function that returns 1 if the i -th bi-gram output by the model is present
 1209 in the True Top n bi-grams, and 0 otherwise,
 - 1210 • True_Top_n represents the set of “good” bi-grams, which in our case is the set of the top n
 1211 scoring bi-grams from the final model step.

1212 **Total mass of bi-grams.** In Section H, we use the total mass as a metric to measure the cumulative
 1213 probabilities of bi-grams from the top 1K bi-grams, weighted by an empirical uni-gram distribution
 1214 derived from real data. Formally, it is given by: Total Mass = $\sum_{(z_1, z_2) \in \text{Top-1K}} \mathbb{P}_{e_t}(z_2|z_1) \mathbb{P}_{\mathcal{D}}(z_1)$
 1215 where:

- 1216
- 1217 • e_t is the embedding-unembedding path at the t -th pre-training step,
 - 1218 • (z_1, z_2) are the bi-grams being considered,
 - 1219 • $\mathbb{P}_{e_t}(z_2|z_1)$ is the probability assigned by the model e_t (the embedding-unembedding path)
 1220 for the token z_2 given token z_1 ,
 - 1221 • $\mathbb{P}_{\mathcal{D}}(z_1)$ is the probability of z_1 under the empirical distribution \mathcal{D} , which is the uni-gram
 1222 probability given by the Infini-gram API (Liu et al., 2024) on the Dolma dataset (Soldaini
 1223 et al., 2024) (the dataset used to pretrain the model checkpoints).

1224 This metric is designed to evaluate how much “correc” probability mass the model checkpoints
 1225 assign to bi-grams (z_1, z_2) , taking into account the empirical uni-gram probability of z_1 . It provides
 1226 insight into how well the model aligns with the empirical distribution of real-world data during the
 1227 pretraining process.

1228

G CASE STUDY 1: ANALYZING LLM INTERNALS WITH JET LENS AND JET 1229 PATHS (ADDITIONAL RESULTS)

1230

G.1 ADDITIONAL PLOTS OF JET LENSES

1231 See plots Figures 7 to 17. The details for obtaining the jet lens plots can be found in . Note that
 1232 for iterative lenses the last block coincides with the model logits for all k by design. We omit the
 1233 iterative lens for GPT2-large for $k = 2$ due to low cosine similarity.

1242

1243

1244

1245

1246

1247

1248

1249

1250

1251

1252

1253

1254

1255

1256

1257

1258

1259

1260

1261

1262

1263

Figure 7: Iterative jet lens ($k = 0$), equivalent to logit lens (nostalgebraist, 2021b), applied over GPT-Neo-2.7B with the input sentence “new simple neural architecture, the Transformer”.

1266

1267

1268

1269

1270

1271

1272

1273

1274

1275

1276

1277

1278

1279

1280

1281

1282

1283

1284

1285

1286

1287

1288

1289

1290

Figure 8: Iterative jet lens ($k = 1$), applied over GPT-Neo-2.7B with the input sentence “new simple neural architecture, the Transformer”.

1291

1292

1293

1294

1295

	new	simple	neural	architecture	,	the	Trans	former
Block 1	Supporters	Supporters	Supporters	Supporters	Supporters	Supporters	Supporters	Supporters
Block 2	Supporters	Supporters	Supporters	Supporters	Supporters	Supporters	Supporters	Supporters
Block 3	Supporters	Supporters	Supporters	Supporters	Supporters	Supporters	Supporters	Supporters
Block 4	Supporters	Supporters	Supporters	Supporters	Supporters	Supporters	Supporters	Supporters
Block 5	Supporters	Supporters	Supporters	Supporters	Supporters	Supporters	Supporters	Supporters
Block 6	Supporters	Supporters	Supporters	Supporters	Supporters	Supporters	Supporters	Supporters
Block 7	Supporters	Supporters	Supporters	Supporters	Supporters	Supporters	Supporters	Supporters
Block 8	Supporters	Supporters	Supporters	Supporters	Supporters	Supporters	Supporters	Supporters
Block 9	Supporters	Supporters	Supporters	Supporters	Supporters	Supporters	Supporters	Supporters
Block 10	Supporters	Supporters	Supporters	Supporters	Supporters	Supporters	Supporters	Supporters
Block 11	Supporters	Supporters	Supporters	Supporters	Supporters	Supporters	Supporters	Supporters
Block 12	Supporters	Supporters	Supporters	Supporters	Supporters	Supporters	Supporters	Supporters
Block 13	Supporters	Supporters	Supporters	Supporters	Supporters	Supporters	Supporters	Supporters
Block 14	Supporters	Supporters	Supporters	Supporters	Supporters	Supporters	Supporters	Supporters
Block 15	Supporters	Supporters	Supporters	Supporters	Supporters	Supporters	Supporters	Supporters
Block 16	Supporters	Supporters	Supporters	Supporters	Supporters	Supporters	Supporters	Supporters
Block 17	Supporters	Supporters	Supporters	Supporters	Supporters	Supporters	Supporters	Supporters
Block 18	Supporters	Supporters	Supporters	Supporters	Supporters	Supporters	Supporters	Supporters
Block 19	Supporters	Supporters	Supporters	Supporters	Supporters	Supporters	Supporters	Supporters
Block 20	Supporters	Supporters	Supporters	Supporters	Supporters	Supporters	Supporters	Supporters
Block 21	Supporters	Supporters	Supporters	Supporters	Supporters	Supporters	Supporters	Supporters
Block 22	Supporters	Supporters	Supporters	Supporters	Supporters	Supporters	Supporters	Supporters
Block 23	Supporters	Supporters	Supporters	Supporters	Supporters	Supporters	Supporters	Supporters
Block 24	Supporters	Supporters	Supporters	Nonetheless	Nonetheless	Nonetheless	Nonetheless	Nonetheless
Block 25	Supporters	Supporters	Supporters	Attempts	Attempts	Attempts	Attempts	Attempts
Block 26	Supporters	Supporters	Supporters	Attempts	Attempts	Attempts	Attempts	Attempts
Block 27	Supporters	Supporters	Supporters	Attempts	Attempts	Attempts	Attempts	Attempts
Block 28	Supporters	Supporters	Supporters	Attempts	Attempts	Attempts	Attempts	Attempts
Block 29	foreseen	Supporters	Supporters	foreseen	foreseen	foreseen	foreseen	foreseen
Block 30	foreseen	Supporters	Supporters	Attempts	foreseen	foreseen	foreseen	foreseen
Block 31	Supporters	Supporters	Supporters	for	the	aminer	former	,
Block 32	—	—	network	for	which	neural	former	,

	Logits	—	—	network	for	which	neural	former	,
Block 1	—	—	—	—	—	—	—	—	,
Block 2	Supporters	ton	network	for	which	first	former	,	,
Block 3	Supporters	ton	network	for	which	first	former	,	,
Block 4	Supporters	ton	network	for	which	first	former	,	,
Block 5	Supporters	ton	network	for	which	first	former	,	,
Block 6	Supporters	ton	network	for	which	first	former	,	,
Block 7	Supporters	ton	network	for	which	first	former	,	,
Block 8	Supporters	ton	network	for	which	first	former	,	,
Block 9	Supporters	ton	network	for	which	first	former	,	,
Block 10	Supporters	ton	network	for	which	first	former	,	,
Block 11	Supporters	ton	network	for	which	first	former	,	,
Block 12	Supporters	ton	network	for	which	first	former	,	,
Block 13	Supporters	ton	network	for	which	first	former	,	,
Block 14	Supporters	ton	network	for	which	first	former	,	,
Block 15	Supporters	ton	network	for	which	first	former	,	,
Block 16	Supporters	ton	network	for	which	first	former	,	,
Block 17	Supporters	ton	network	for	which	first	former	,	,
Block 18	Supporters	ton	network	for	which	first	former	,	,
Block 19	Supporters	ton	network	for	which	first	former	,	,
Block 20	Supporters	ton	network	for	which	first	former	,	,
Block 21	Supporters	ton	network	for	which	first	former	,	,
Block 22	Supporters	ton	network	for	which	first	former	,	,
Block 23	Supporters	ton	network	for	which	first	former	,	,
Block 24	Supporters	ton	network	for	which	so	former	,	,
Block 25	Supporters	ton	network	for	which	first	former	,	,
Block 26	Supporters	ton	network	for	which	first	former	,	,
Block 27	Supporters	ton	network	for	which	first	former	,	,
Block 28	Supporters	ton	network	for	which	first	former	,	,
Block 29	foreseen	ton	network	for	which	first	former	,	,
Block 30	Supporters	—	network	for	which	first	former	,	,
Block 31	Supporters	—	network	for	which	first	former	,	,
Block 32	—	—	network	for	which	neural	former	,	,

1296

1297

1298

1299

	new	simple	neural	architecture	,	the	Trans	former
Block 1	the	—	nets	!:	ag!"	ag!"	former	:
Block 2	the	—	network	output	ag!"	ag!"	former	—
Block 3	the	—	network	for	trained	Conv	former	—
Block 4	the	—	network	for	the	Conv	former	,
Block 5	the	—	network	for	the	neural	former	,
Block 6	the	—	network	for	the	neural	former	,
Block 7	the	—	network	for	the	architecture	former	,
Block 8	the	—	network	for	the	architecture	former	,
Block 9	the	—	network	for	the	architecture	former	,
Block 10	the	—	network	for	the	architecture	former	,
Block 11	the	—	network	for	the	architecture	former	,
Block 12	the	—	network	for	the	architecture	former	,
Block 13	the	—	network	for	the	architecture	former	,
Block 14	the	—	network	for	the	neural	former	,
Block 15	the	—	network	for	the	neural	former	,
Block 16	the	—	network	for	the	neural	former	,
Block 17	the	—	network	for	the	neural	former	,
Block 18	the	—	network	for	the	neural	former	,
Block 19	the	—	network	for	the	neural	former	,
Block 20	the	—	network	for	the	neural	former	,
Block 21	the	—	network	for	the	neural	former	,
Block 22	the	—	network	for	the	neural	former	,
Block 23	the	—	network	for	the	neural	former	,
Block 24	the	—	network	for	the	neural	former	,
Block 25	the	—	network	for	the	neural	former	,
Block 26	the	—	network	for	the	neural	former	,
Block 27	the	—	network	for	the	neural	former	,
Block 28	the	—	network	for	the	neural	former	,
Block 29	the	—	network	for	the	neural	former	,
Block 30	the	—	network	for	and	neural	former	,
Block 31	,	—	network	for	and	neural	former	,
Block 32	—	—	network	for	which	neural	former	,

1316

Figure 9: Iterative jet lens ($k = 2$), applied over GPT-Neo-2.7B with the input sentence “new simple neural architecture, the Transformer”

1317

1318

1319

1320

1321

1322

1323

1324

1325

	new	simple	neural	architecture	,	the	Trans	former
Block 1	bie	simple	neural	architecture	and	the	fig	former
Block 2	bie	simple	neural	architecture	and	main	ient	former
Block 3	bie	simple	neural	architecture	and	new	ient	former
Block 4	bie	way	neural	architecture	and	first	ient	titan
Block 5	bie	way	networks	architecture	and	next	ient	Prime
Block 6	bie	enough	networks	architecture	and	next	ient	Matrix
Block 7	href	enough	networks	architecture	and	first	ient	Prime
Block 8	itunes	enough	neural	architecture	which	first	ient	Revolution
Block 9	,	enough	neural	architecture	which	first	ient	Prime
Block 10	,	enough	network	architecture	which	first	ient	Revolution
Block 11	,	enough	network	model	which	only	ient	Pro
Block 12	,	enough	network	architecture	which	only	ient	Pro
Block 13	,	enough	network	model	which	first	ient	Pro
Block 14	,	enough	network	model	which	first	ient	Pro
Block 15	,	enough	network	model	which	only	ient	Pro
Block 16	,	—	network	model	which	only	ient	Revolution
Block 17	,	—	system	model	which	only	ient	Prime
Block 18	,	—	system	model	which	only	ient	Prime
Block 19	,	—	system	model	which	only	ient	Prime
Block 20	,	—	system	model	which	only	ient	Prime
Block 21	,	—	system	model	which	only	ient	Prime
Block 22	,	—	network	model	which	only	ient	Prime
Block 23	,	ton	network	model	which	only	ient	Prime
Block 24	,	ton	network	model	which	only	ient	Prime
Block 25	,	ton	network	model	which	first	ient	Prime
Block 26	,	ton	network	model	which	only	ient	Prime
Block 27	,	ton	network	for	which	first	ient	Prime
Block 28	,	—	network	“	which	only	ient	Prime
Block 29	,	—	network	“	which	neural	ient	Prime
Block 30	,	“	network	“	which	neural	ient	,
Block 31	,	“	network	“	which	neural	ient	,
Block 32	,	“	network	“	which	neural	ient	,
Block 33	,	“	network	for	which	neural	ient	,
Block 34	,	“	network	“	which	neural	ient	,
Block 35	,	“	network	“	which	neural	c	,
Block 36	—	“	network	“	which	neural	c	,

1344

1345

Figure 10: Iterative jet lens ($k = 0$), equivalent to Logit Lens (nostalggebraist, 2021b), applied over GPT-2-large with the input sentence “new simple neural architecture, the Transformer”.

1346

1347

1348

1349

1350

1351

1352

	new	_simple	neural	architecture	,	the	_Trans	former
Block 1	bie	"	network		which	neural	c	is
Block 2	bie	"	network	,	which	neural	c	is
Block 3	bie	"	network	,	which	neural	c	is
Block 4	-	"	network	,	which	neural	c	is
Block 5	-	"	network	,	which	neural	c	is
Block 6	-	"	network	,	which	neural	c	is
Block 7	-	"	network	,	which	neural	c	is
Block 8	-	"	network	,	which	neural	c	is
Block 9	-	"	network	,	which	neural	c	is
Block 10	,	"	network	,	which	neural	c	is
Block 11	,	"	network	,	which	neural	c	is
Block 12	,	"	network	,	which	neural	c	,
Block 13	,	"	network	,	_where	neural	c	,
Block 14	,	"	network	,	_and	neural	c	,
Block 15	,	"	network	,	_and	neural	c	,
Block 16	,	"	network	,	_and	neural	c	,
Block 17	,	"	network	,	and	neural	c	,
Block 18	,	"	network	,	and	neural	c	,
Block 19	,	"	network	,	and	neural	c	,
Block 20	,	"	network	,	and	neural	c	,
Block 21	,	"	network	,	and	neural	c	,
Block 22	,	"	network	,	and	neural	c	,
Block 23	,	"	network	,	the	neural	c	,
Block 24	,	"	network	,	and	neural	c	,
Block 25	,	"	network	,	and	neural	c	,
Block 26	,	"	network	,	and	neural	c	,
Block 27	,	"	network	,	and	neural	c	,
Block 28	,	"	network	,	and	neural	c	,
Block 29	,	"	network	,	and	human	c	,
Block 30	,	"	network	,	and	same	c	,
Block 31	,	"	network	,	and	same	c	,
Block 32	,	"	network	,	and	same	c	,
Block 33	,	"	network	,	and	neural	c	,
Block 34	,	"	network	,	which	neural	c	,
Block 35	-	"	network	,	which	neural	c	,
Block 36	-	"	network	,	which	neural	c	,
Logits	-	"	network	,	which	neural	c	,

Figure 11: Iterative jet lens ($k = 1$), applied over GPT-2-large with the input sentence “new simple neural architecture, the Transformer”

1374

1375

1376

1377

1378

	new	_simple	neural	architecture	,	the	_Trans	former
Block 1 (4.40%)	, (6.62%)	simple (3.91%)	neural (4.42%)	architecture (3.97%)	, which (4.07%)	same (4.37%)	cend (3.93%)	former (3.91%)
Block 2 (4.15%)	, (6.59%)	retro (3.85%)	prog (4.32%)	error (3.74%)	, including (3.93%)	resulting (4.14%)	ference (3.69%)	Robo (2.99%)
Block 3 (4.23%)	, (6.59%)	ova (4.13%)	Matter (4.12%)	killer (3.51%)	, which (4.09%)	AVG (4.01%)	em (3.56%)	Mars (3.91%)
Block 4 (4.11%)	, (6.59%)	the (6.59%)	reg (3.53%)	lect (4.37%)	OX (3.68%)	found (4.05%)	netflix (4.09%)	Charge (2.95%)
Block 5 (6.11%)	, (6.59%)	ware (3.54%)	product (3.68%)	towards (3.70%)	evolution (3.88%)	ones (3.74%)	it (2.03%)	A@ (3.69%)
Block 6 (0.91%)	, (6.58%)	ies (3.59%)	_networks (4.13%)	_developed (3.45%)	_developed (3.55%)	_Mehran (3.45%)	itition (3.54%)	_Mant (0.57%)
Block 7 (4.06%)	, (6.55%)	face (3.75%)	_studies (3.86%)	based (3.52%)	hackers (3.76%)	Turing (3.73%)	Series (2.97%)	_Sutte (3.83%)
Block 8 (4.06%)	, (6.42%)	key (3.83%)	model (4.18%)	based (3.53%)	requiring (3.49%)	algorithm (4.14%)	ient (3.62%)	_II (3.25%)
Block 9 (4.09%)	, (7.45%)	_cluster (4.08%)	model (3.69%)	_test (3.40%)	_which (3.11%)	_neural (3.55%)	verse (3.82%)	_Cube (3.66%)
Block 10 (10.50%)	, (16.50%)	lists (9.61%)	g (4.99%)	_of (16.60%)	_which (11.47%)	_neural (5.79%)	_neural (3.50%)	_is (15.56%)
Block 11 (25.30%)	, (16.96%)	" (27.59%)	_networks (28.89%)	" (24.52%)	_the (26.92%)	_new (29.14%)	m (22.95%)	_neural (25.40%)
Block 12 (25.13%)	, (6.56%)	net (29.35%)	, (26.40%)	the (27.77%)	the (29.85%)	c (25.27%)		(27.23%)
Logits	,	-	network	that	which	neural	ient	is
Expan. (1.000)	,	-	network	of	which	"	-	is

Figure 12: Joint jet lens with learnable weightings ($k = 0$), applied over GPT2 with the input sentence “new simple neural architecture, the Transformer”

1386

1387

1388

1389

1390

1391

1392

	new	_simple	neural	architecture	,	the	_Trans	former
Block 1 (15.30%)	, (7.49%)	" (16.78%)	_networks (16.96%)	, (18.37%)	_neural (14.61%)	_neural (14.05%)	verse (16.45%)	Neural (17.73%)
Block 2 (4.57%)	, (13.81%)	json (3.21%)	_networks (3.29%)	_model (3.46%)	_which (3.11%)	_neural (3.02%)	cend (3.23%)	Neural (3.45%)
Block 3 (4.49%)	, (14.25%)	ton (3.25%)	_networks (2.82%)	_architecture (3.32%)	_neural (3.10%)	_neural (3.00%)	porter (3.03%)	Neural (3.17%)
Block 4 (4.10%)	, (11.55%)	ton (3.28%)	_networks (3.27%)	_leveraging (3.19%)	_synt (3.04%)	_neural (2.98%)	verse (2.90%)	Neural (2.57%)
Block 5 (4.02%)	, (9.58%)	ton (3.05%)	_networks (3.25%)	_algorithm (3.45%)	_which (3.14%)	_neural (2.99%)	mitter (3.24%)	Neural (3.47%)
Block 6 (3.02%)	, (2.75%)	_linkage (2.65%)	_net (3.04%)	_algorithm (3.26%)	_detecting (2.94%)	_neural (2.80%)	cend (3.30%)	Neural (3.45%)
Block 7 (2.91%)	, (2.98%)	_teleportation (2.78%)	_nets (3.19%)	_approach (3.24%)	_specifically (2.49%)	_cortex (2.58%)	genic (3.07%)	Cortex (2.95%)
Block 8 (4.60%)	, (3.10%)	net (7.64%)	_network (2.63%)	_platform (2.62%)	_neural (4.81%)	_participant (9.06%)	cription (3.50%)	Neural (3.45%)
Block 9 (7.44%)	, (3.10%)	uri (5.60%)	_network (7.77%)	_intelligence (4.86%)	_torch (14.64%)	_welcoming (13.48%)	Secure (7.21%)	_conv (2.83%)
Block 10 (15.04%)	, (13.99%)	widget (14.80%)	_network (16.20%)	_None (13.05%)	_Bund (15.37%)	_safest (14.72%)	cend (16.11%)	_disabling (16.06%)
Block 11 (16.50%)	, (3.19%)	ton (18.47%)	_network (18.79%)	_architecture (20.49%)	_which (16.34%)	_neural (15.62%)	istor (18.84%)	Att@ (20.28%)
Block 12 (18.00%)	, (14.21%)	network (18.49%)	that (20.68%)	which (16.41%)	neural (15.70%)	ient (19.11%)	is (20.60%)	
Logits	,	-	network	that	which	neural	ient	is
Expan. (1.000)	akings	json	_networks	framework	_neural	cend	Neural	

Figure 13: Joint jet lens with learnable weightings ($k = 1$), applied over GPT2 with the input sentence “new simple neural architecture, the Transformer”

1400

1401

1402

1403

1404

1405

1406

1407

1408

1409

1410

1411

1412

1413

1414

1415

1416

1417

1418

1419

1420

1421

1422

1423

1424

1425

1426

1427

1428

1429

1430

1431

1432

1433

1434

1435

1436

1437

1438

1439

1440

1441

1442

1443

1444

1445

1446

1447

1448

1449

1450

1451

1452

1453

1454

1455

1456

1457

	new	simple	neural	architecture	the	Trans	former
Block 1 (3.58%)	Supporters (1.55%)	Supporters (3.24%)	Supporters (3.46%)	Supporters (3.96%)	Supporters (5.09%)	Supporters (3.52%)	Supporters (3.88%)
Block 2 (2.33%)	foreseen (1.61%)	foreseen (2.97%)	foreseen (1.15%)	Introduced (3.96%)	foreseen (1.69%)	foreseen (1.54%)	Supporters (2.56%)
Block 3 (2.07%)	Amid (1.65%)	Supporters (2.01%)	Across (1.32%)	gewer (1.34%)	Supporters (3.66%)	Supporters (2.93%)	Supporters (3.67%)
Block 4 (1.57%)	_impovert (1.97%)	_unpop (2.18%)	_unpop (1.46%)	_impovert (1.33%)	_impovert (1.39%)	_impovert (1.71%)	Supporters (1.03%)
Block 5 (1.47%)	Attempts (1.76%)	_municip (2.15%)	_inst (1.45%)	_linen (1.29%)	_similar (1.32%)	pelting (1.38%)	_uphe (1.27%)
Block 6 (1.45%)	Residents (1.76%)	_attlet (2.17%)	tha (1.44%)	_twent (1.34%)	_way (1.05%)	ters (1.40%)	_linen (1.13%)
Block 7 (3.57%)	Ironically (1.63%)	cenote (2.74%)	wrap (3.78%)	_book (5.71%)	_junkie (1.22%)	_equivalent (2.63%)	_hollow (4.36%)
Block 8 (4.63%)	Supporters (1.61%)	linura (3.91%)	vantage (3.03%)	anios (5.48%)	foreseen (6.13%)	ileen (4.53%)	assador (6.59%)
Block 9 (3.14%)	Ironically (1.65%)	ergusion (2.00%)	certain (2.53%)	OUR (1.28%)	_local (3.54%)	ergusion (1.80%)	enter (5.43%)
Block 10 (1.73%)	foreseen (1.65%)	foreseen (2.01%)	Engineers (1.20%)	Engineers (2.88%)	asury (1.19%)	thinkable (1.40%)	Attempts (2.53%)
Block 11 (1.71%)	likely (1.57%)	extremely (1.48%)	aples (1.18%)	_screenplay (1.29%)	earances (1.30%)	earances (4.13%)	uddently (0.96%)
Block 12 (4.53%)	Ironically (1.73%)	Phones (3.91%)	ADVERTISEMENT (4.39%)	ADVERTISEMENT (6.03%)	isively (1.65%)	_Bld (4.46%)	ADVERTISEMENT (4.08%)
Block 13 (2.89%)	_a (1.68%)	at (2.83%)	imbistave (1.33%)	rone (1.28%)	OTOS (5.38%)	ppard (3.08%)	aj (5.76%)
Block 14 (2.91%)	foreseen (1.66%)	ADVERTISEMENT (1.83%)	Marginal (3.82%)	shell (1.32%)	_Appalach (1.33%)	Caucasse (4.66%)	_still (5.47%)
Block 15 (1.47%)	ormons (1.78%)	_confir (1.89%)	uring (3.34%)	urel (1.25%)	_Ad (1.38%)	Caucas (1.68%)	lineman (1.25%)
Block 16 (3.08%)	Against (1.82%)	folios (1.93%)	@ (0.49%)	thinkable (3.49%)	tsun (1.26%)	D (4.65%)	_topple (1.22%)
Block 17 (2.89%)	urste (1.38%)	united (4.40%)	ortunate (3.72%)	hub (1.21%)	par (4.49%)	Ortment (1.51%)	arch (3.88%)
Block 18 (5.12%)	foreseen (1.63%)	Supporters (4.53%)	Nonetheless (6.62%)	Ironically (5.07%)	Thankfully (5.66%)	Shorty (4.52%)	errem (4.91%)
Block 19 (2.06%)	_enough (4.91%)	_enough (4.91%)	og (3.58%)	for (5.69%)	incenty (1.08%)	incenty (2.75%)	ombies (1.21%)
Block 20 (5.48%)	C (2.06%)	C (5.07%)	Just (7.05%)	C (6.61%)	Attempts (6.51%)	parallel (4.49%)	extreme (0.01%)
Block 21 (1.46%)	ription (1.60%)	ription (3.15%)	_Playoffs (1.40%)	isdom (1.08%)	_frontrunner (1.36%)	_frontrunner (1.69%)	phabet (1.21%)
Block 22 (4.55%)	_in (3.36%)	_inst (2.59%)	_two (7.65%)	one (6.98%)	which (6.97%)	_one (4.56%)	pered (1.06%)
Block 23 (5.21%)	, (4.80%)	jl (5.23%)	_10 (1.39%)	je (0.26%)	while (6.33%)	_point (4.57%)	albeit (1.15%)
Block 24 (6.13%)	_a (5.62%)	_m (5.26%)	_first (7.18%)	for (7.33%)	the (7.33%)	_so (4.70%)	B (8.21%)
Block 25 (1.55%)	foreseen (1.67%)	acy (2.14%)	enthias (1.49%)	_ained (1.35%)	trainers (1.43%)	_subreddits (1.74%)	reveng (5.96%)
Block 26 (2.61%)	- (6.25%)	simple (2.08%)	simple (5.95%)	ername (1.30%)	haat (1.34%)	_satell (1.74%)	_trainer (1.27%)
Block 27 (2.65%)	8G (7.40%)	8G (5.49%)	DSM (1.35%)	head (1.30%)	dayName (1.38%)	igsw (1.02%)	headphone (1.17%)
Block 28 (2.39%)	fps (8.56%)	> (12.30%)	_On (1.42%)	taics (1.30%)	_rsec (1.41%)	_unbelieve (1.75%)	_nostalg (1.30%)
Block 29 (1.97%)	8G (7.17%)	convol (2.18%)	ricanes (1.47%)	_Gujar (1.25%)	acer (0.18%)	cffl (1.74%)	_reminis (1.28%)
Block 30 (1.84%)	8G (4.01%)	_anned (2.24%)	_Urve (1.49%)	overwhel (1.37%)	?? (1.43%)	20439 (1.78%)	_negoli (1.29%)
Block 31 (6.41%)	!! (8.40%)	8G (2.57%)	_greets (1.35%)	_enter (1.80%)	\\ (4.44%)	\\ (6.14%)	* (5.27%)
Block 32 (5.64%)	8G (9.55%)	?? (4.42%)	8G (2.29%)	8G (5.37%)	8G (6.35%)	\\' (9.03%)	*\\yu (3.34%)
Logits	Expan. (0.977)	the	and	network	for	which	former
			-	-	-	-	-

Figure 14: Joint jet lens with learnable weightings ($k = 0$), applied over GPT-Neo-2.7B with the input sentence “new simple neural architecture, the Transformer”

	new	simple	neural	architecture	the	Trans	former
Block 1 (7.36%)	(3.40%)	ton (8.06%)	network (8.57%)	-for (8.22%)	_which (7.51%)	_first (7.30%)	former (7.43%)
Block 2 (4.83%)	(2.39%)	(5.23%)	_network (6.63%)	for (4.98%)	_which (4.60%)	_neural (4.77%)	former (5.09%)
Block 3 (1.31%)	_File (1.62%)	(1.29%)	_network (1.31%)	_for (1.28%)	_which (1.25%)	CNN (1.22%)	former (1.20%)
Block 4 (7.81%)	_impovert (5.74%)	_unpop (8.48%)	_impovert (8.76%)	_impovert (8.45%)	_impovert (7.67%)	_Neural (7.51%)	Networks (8.45%)
Block 5 (1.79%)	User (5.29%)	(1.31%)	_network (1.30%)	for (1.29%)	_which (1.29%)	_neural (1.26%)	former (1.25%)
Block 6 (1.79%)	Instance (5.33%)	(1.33%)	_network (1.31%)	for (1.29%)	_which (1.26%)	_neural (1.23%)	former (1.23%)
Block 7 (1.59%)	File (3.56%)	(1.37%)	_network (1.36%)	for (1.33%)	_which (1.28%)	_neural (1.24%)	former (1.25%)
Block 8 (1.70%)	Supporters (5.02%)	(1.29%)	_network (1.28%)	for (1.25%)	_which (1.24%)	_Neural (1.17%)	former (1.12%)
Block 9 (1.77%)	Enlarge (5.04%)	(1.37%)	_network (1.37%)	for (1.32%)	_which (1.26%)	_neural (1.23%)	former (1.25%)
Block 10 (4.41%)	foreseen (5.36%)	(5.77%)	_network (6.19%)	for (5.99%)	_which (1.15%)	_neural (0.93%)	former (2.45%)
Block 11 (1.31%)	(1.90%)	(1.30%)	_network (1.29%)	for (1.20%)	_which (1.18%)	_neural (1.19%)	former (1.19%)
Block 12 (6.21%)	(1.74%)	(1.11%)	_network (1.17%)	for (1.10%)	_which (1.16%)	_neural (1.15%)	former (1.07%)
Block 13 (1.37%)	(1.94%)	(1.36%)	_network (1.35%)	for (1.32%)	_which (1.23%)	former (1.21%)	former (1.23%)
Block 14 (1.22%)	(1.82%)	(1.18%)	_network (1.22%)	for (1.12%)	_which (1.15%)	_neural (1.09%)	former (1.04%)
Block 15 (1.34%)	(1.90%)	(1.33%)	_network (1.31%)	for (1.29%)	_which (1.21%)	_neural (1.20%)	former (1.20%)
Block 16 (1.31%)	(1.91%)	(1.28%)	_network (1.28%)	for (1.24%)	_which (1.18%)	_neural (1.19%)	model (1.23%)
Block 17 (1.31%)	(1.90%)	(1.29%)	_network (1.28%)	for (1.26%)	_which (1.14%)	_neural (1.12%)	former (1.16%)
Block 18 (4.55%)	(1.65%)	(5.16%)	_network (3.55%)	for (5.49%)	_which (6.28%)	_neural (6.05%)	former (5.05%)
Block 19 (1.24%)	(1.84%)	(1.23%)	_network (1.17%)	for (1.18%)	_which (1.23%)	_neural (0.97%)	former (1.10%)
Block 20 (1.36%)	C (1.84%)	(2.30%)	_network (1.16%)	for (4.21%)	_which (6.29%)	_neural (5.89%)	former (2.70%)
Block 21 (1.87%)	(1.80%)	(1.21%)	_network (1.12%)	for (1.15%)	_which (3.82%)	_neural (3.71%)	former (1.10%)
Block 22 (4.81%)	(1.91%)	infographic (8.14%)	_network (3.56%)	output (5.92%)	_which (6.89%)	_neural (6.76%)	former (1.57%)
Block 23 (2.01%)	(1.91%)	(1.14%)	_network (1.40%)	learns (1.38%)	_which (3.94%)	_Conv (3.99%)	former (1.14%)
Block 24 (6.02%)	(1.94%)	infographic (8.04%)	_network (1.20%)	unve (8.00%)	_unve (7.47%)	_Neural (7.02%)	model (3.53%)
Block 25 (1.19%)	(1.87%)	(1.19%)	_network (1.09%)	for (1.22%)	_which (0.96%)	8G (1.07%)	model (4.98%)
Block 26 (1.55%)	(1.89%)	(1.18%)	_network (1.18%)	called (1.22%)	_which (1.25%)	Conv (1.09%)	former (2.57%)
Block 27 (1.23%)	(1.93%)	ton (3.53%)	_network (1.09%)	for (1.21%)	_which (0.99%)	_model (1.13%)	former (6.67%)
Block 28 (2.76%)	(1.73%)	json (1.02%)	_network (3.49%)	for (1.84%)	_which (0.95%)	_Neural (3.31%)	former (6.31%)
Block 29 (3.22%)	8G (6.01%)	(1.32%)	_network (1.00%)	for (1.01%)	_and (1.74%)	_neural (1.90%)	former (7.25%)
Block 30 (6.24%)	8G (6.04%)	(3.56%)	_network (7.34%)	for (5.45%)	_which (6.05%)	_neural (6.14%)	former (7.30%)
Block 31 (7.76%)	!! (5.96%)	(8.27%)	_network (6.68%)	for (8.36%)	the (7.67%)	Conv (7.46%)	former (7.35%)
Block 32 (7.84%)	8G (5.81%)	?? (8.35%)	_network (8.78%)	(8.43%)	_and (7.70%)	_neural (7.51%)	former (7.57%)
Logits	Expan. (0.993)	-	-	network	for	which	former
			-	-	-	-	-

Figure 15: Joint jet lens with learnable weightings ($k = 1$), applied over GPT-Neo-2.7B with the input sentence “new simple neural architecture, the Transformer”

1458

1459

1460

1461

	new	_simple	_neural	_architecture	-	_the	_trans	former
Block 1 (3.19%)	bie (4.48%)	_simple (4.99%)	_neural (0.98%)	_architecture (1.08%)	-	_the (5.85%)	_fig (2.07%)	former (1.01%)
Block 2 (1.61%)	arrivals (2.43%)	tons (1.22%)	_rack (3.83%)	_model (1.07%)	-	_the (1.01%)	_main (1.01%)	ient (3.10%)
Block 3 (2.49%)	entry (0.53%)	fitting (5.41%)	_clusters (0.95%)	_det (1.34%)	-	_thanks (0.99%)	_second (1.00%)	cription (0.97%)
Block 4 (3.02%)	ties (3.47%)	private (5.64%)	_env (5.41%)	_clusters (1.18%)	-	_aspirin (1.09%)	_hypothesis (1.08%)	barrier (1.86%)
Block 5 (1.75%)	mansion (3.47%)	_Transcript (1.03%)	ous (2.48%)	_suit (1.35%)	-	_chuk (1.11%)	_script (5.55%)	Mundi (0.75%)
Block 6 (1.84%)	_Probates (2.46%)	_Bald (1.48%)	ter (0.99%)	_sche (1.21%)	-	_hi (1.11%)	_hi (0.18%)	ione (5.34%)
Block 7 (2.51%)	DERR (2.47%)	_ap (1.62%)	_weed (3.21%)	inea (1.19%)	-	_Y* (1.02%)	_glass (1.17%)	aways (4.96%)
Block 8 (1.80%)	-	_Ball (1.04%)	_experiments (0.89%)	MIT (1.21%)	-	_mice (1.06%)	_fts (1.16%)	_system (4.48%)
Block 9 (1.79%)	-	(2.37%)	-	-	-	-	_rock (5.75%)	con (0.97%)
Block 10 (2.17%)	-	(2.38%)	tested (1.09%)	(6.21%)	-	-	-	boxeo (0.96%)
Block 11 (1.20%)	-	(2.38%)	azon (1.09%)	ea (1.20%)	-	-	-	ter (0.98%)
Block 12 (1.17%)	-	(2.20%)	Think (1.05%)	_dish (0.86%)	-	-	-	_INS (0.76%)
Block 13 (1.88%)	-	(2.22%)	_and (2.77%)	ourt (4.11%)	-	-	-	_Drive (1.80%)
Block 14 (1.60%)	-	(2.22%)	aly (1.06%)	_underestimated (0.97%)	-	-	-	_Revised (0.95%)
Block 15 (2.19%)	-	(2.24%)	-	(4.45%)	-	-	-	_Pre (1.00%)
Block 16 (2.24%)	-	(2.26%)	_image (5.83%)	_cell (4.89%)	-	-	-	_Re (1.0%)
Block 17 (1.72%)	-	(2.27%)	AI (1.11%)	_formulation (0.96%)	-	-	-	_prob (1.02%)
Block 18 (1.54%)	-	(2.21%)	bond (1.06%)	(9.1%)	-	-	-	_Neural (0.85%)
Block 19 (2.17%)	-	(2.13%)	cross (3.75%)	_proceeds (0.61%)	-	-	-	_Trainer (5.29%)
Block 20 (2.64%)	-	(3.62%)	-	(0.98%)	-	-	-	_modular (1.08%)
Block 21 (1.27%)	-	(3.47%)	-	(0.97%)	-	-	-	_Space (0.99%)
Block 22 (3.08%)	-	(3.56%)	types (0.98%)	Turing (2.15%)	-	-	-	_brand (0.78%)
Block 23 (3.17%)	-	(3.59%)	tv (1.07%)	blade (0.96%)	-	-	-	_Quest (0.91%)
Block 24 (5.36%)	-	(3.89%)	prayers (5.37%)	Turing (6.05%)	-	-	-	Shares (0.96%)
Block 25 (2.84%)	-	(3.80%)	_complex (0.86%)	surgery (0.93%)	-	-	-	Jost (0.81%)
Block 26 (5.61%)	-	(3.83%)	dot (0.73%)	Turing (6.16%)	-	-	-	_parallel (0.93%)
Block 27 (4.91%)	-	(3.64%)	? (7.12%)	_algorithm (2.21%)	-	-	-	_Shans (0.96%)
Block 28 (3.91%)	-	(2.94%)	_solution (0.91%)	_simulation (4.19%)	-	-	-	_Fly (1.73%)
Block 29 (4.07%)	-	(1.51%)	! (6.69%)	_network (2.58%)	-	-	-	_letter (1.09%)
Block 30 (5.05%)	-	(1.96%)	AI (5.52%)	_net (5.50%)	-	-	-	adic (0.79%)
Block 31 (5.02%)	-	(2.04%)	-	(6.84%)	-	-	-	Atre (0.87%)
Block 32 (5.00%)	-	(2.06%)	-	(5.21%)	-	-	-	gress (1.06%)
Block 33 (3.65%)	-	(2.08%)	-	(0.83%)	-	-	-	VT (5.74%)
Block 34 (2.57%)	-	(2.10%)	-	(0.10%)	-	-	-	erg (4.52%)
Block 35 (1.67%)	-	(2.12%)	client (1.09%)	.NET (1.00%)	C (3.33%)	-	-	arts (0.83%)
Block 36 (1.28%)	-	(2.69%)	C (1.06%)	gill (1.03%)	C (1.15%)	-	-	scripts (0.93%)
Logits	-	-	-	-	-	-	-	stats (1.02%)
Expan. (0.980)	-	-	-	-	-	-	-	-

1480

Figure 16: Joint jet lens with learnable weightings ($k = 0$), applied over GPT-2-large with the input sentence “new simple neural architecture, the Transformer”

1483

1484

1485

1486

1487

1488

	new	_simple	_neural	_architecture	-	_the	_Trans	former
Block 1 (3.50%)	bie (3.17%)	* (4.75%)	_network (5.93%)	* (6.61%)	-	_which (1.15%)	_neural (1.60%)	c (5.06%)
Block 2 (3.14%)	-	(0.84%)	(4.15%)	_network (5.49%)	-	_which (4.28%)	_neural (4.04%)	c (3.60%)
Block 3 (1.19%)	-	(0.86%)	(0.91%)	_network (0.84%)	-	_which (1.05%)	_neural (2.17%)	c (0.78%)
Block 4 (1.08%)	-	(0.77%)	ton (1.88%)	_network (1.21%)	-	_we (0.96%)	_neural (0.94%)	c (0.75%)
Block 5 (0.98%)	-	(0.74%)	-	(0.93%)	-	-	-	c (1.07%)
Block 6 (1.29%)	-	(3.29%)	-	(1.01%)	-	_network (0.93%)	-	c (1.06%)
Block 7 (1.32%)	-	(3.60%)	-	(1.04%)	-	_network (0.97%)	-	parent (0.89%)
Block 8 (1.35%)	-	(3.71%)	-	(1.05%)	-	_network (0.95%)	-	parent (0.89%)
Block 9 (1.44%)	-	(3.74%)	-	(1.04%)	-	_network (0.83%)	-	parent (0.89%)
Block 10 (1.47%)	-	(3.73%)	-	(1.04%)	-	_network (1.44%)	-	parent (0.93%)
Block 11 (1.36%)	-	(3.71%)	-	(0.98%)	-	_network (1.01%)	-	parent (0.93%)
Block 12 (1.36%)	-	(3.69%)	-	(1.00%)	-	_network (1.04%)	-	parent (0.93%)
Block 13 (1.35%)	-	(3.65%)	-	(1.01%)	-	_network (1.04%)	-	parent (0.93%)
Block 14 (1.31%)	-	(3.61%)	-	(1.00%)	-	_network (1.02%)	-	parent (0.93%)
Block 15 (1.30%)	-	(3.54%)	-	(0.99%)	-	_network (1.03%)	-	parent (0.93%)
Block 16 (1.30%)	-	(3.43%)	-	(1.04%)	-	_network (0.95%)	-	parent (0.93%)
Block 17 (1.28%)	-	(3.36%)	-	(0.97%)	-	_network (0.95%)	-	parent (0.93%)
Block 18 (1.14%)	-	(2.81%)	-	(0.92%)	-	_network (1.00%)	-	parent (0.93%)
Block 19 (0.99%)	-	(0.98%)	-	(0.84%)	-	_network (0.88%)	-	parent (0.93%)
Block 20 (1.53%)	-	(0.95%)	x (0.88%)	-	-	-	-	parent (0.93%)
Block 21 (1.23%)	-	(0.96%)	-	(0.86%)	-	-	-	parent (0.93%)
Block 22 (1.12%)	-	(0.96%)	-	(2.47%)	-	_network (0.88%)	-	parent (0.93%)
Block 23 (2.10%)	-	(0.90%)	stuff (0.79%)	-	-	-	-	parent (0.93%)
Block 24 (3.06%)	-	(0.93%)	(2.25%)	-	-	-	-	parent (0.93%)
Block 25 (3.99%)	= (3.39%)	ton (4.25%)	-	_net (2.85%)	-	(2.19%)	-	parent (0.93%)
Block 26 (1.96%)	Instance (3.52%)	(3.67%)	_network (3.98%)	-	(4.45%)	-	-	parent (0.93%)
Block 27 (1.99%)	-	(3.24%)	tons (5.87%)	_network (4.56%)	-	(5.90%)	-	parent (0.93%)
Block 28 (1.31%)	-	(3.08%)	ton (5.20%)	_network (5.48%)	-	(5.93%)	-	parent (0.93%)
Block 29 (0.04%)	-	(3.27%)	ms (5.80%)	_network (5.64%)	-	(5.22%)	-	parent (0.93%)
Block 30 (4.88%)	-	(3.40%)	kitchen (4.88%)	_network (5.69%)	-	(5.41%)	-	parent (0.93%)
Block 31 (0.31%)	-	(3.61%)	x (6.06%)	_network (5.85%)	-	(6.79%)	-	parent (0.93%)
Block 32 (0.51%)	-	(3.70%)	white (5.66%)	_network (5.56%)	-	(6.49%)	-	parent (0.93%)
Block 33 (0.75%)	-	(3.73%)	-	(6.05%)	-	(6.91%)	-	parent (0.93%)
Block 34 (5.88%)	-	(3.73%)	ton (6.26%)	_network (6.49%)	-	(6.91%)	-	parent (0.93%)
Block 35 (5.77%)	-	(3.74%)	* (6.11%)	_network (6.28%)	-	(6.90%)	-	parent (0.93%)
Block 36 (5.85%)	-	(3.67%)	-	(6.29%)	-	(6.77%)	-	parent (0.93%)
Logits	-	-	-	-	-	-	-	-
Expan. (0.994)	-	-	-	-	-	-	-	-

1508

Figure 17: Joint jet lens with learnable weightings ($k = 1$), applied over GPT-2-large with the input sentence “new simple neural architecture, the Transformer”

1509

1510

1511

1512 Table 5: Several attention heads in the first residual block of *OLMo-7B* and their roles identified with jet tri-
 1513 grams extracted from corresponding jet paths. We also include an example tri-gram captured by each head.

Head Index	2	16	26	30
Role	Math/LaTeX	“for...purposes”	date composition	“into account/consideration ...”
Example 3-gram	(<code>_Lemma, _let, _s</code>)	(<code>_for, _use, _purposes</code>)	(<code>20, 23, _</code>)	(<code>_into, _account, _possible</code>)
$\Delta \text{logit after intervention}$	-0.1570	-0.0019	-0.0093	-0.0001

G.2 ADDITIONAL TABLES OF JET PATHS OF INDIVIDUAL COMPONENTS

1521 Table 5 reports a role identification study on attention heads in the first self-attention of *OLMo-7B*
 1522 using jet tri-grams. Specifically, we find heads associated with math and programming, e.g. head
 1523 1 on Math/Latex; heads promoting digits and dash composition into dates, e.g. head 25; and heads
 1524 constituting phrase templates, e.g. head 15 managing a “for x purposes”, where x is a placeholder.
 1525 To verify the roles we revealed, we further perform preliminary intervention experiments where we
 1526 ablate MLPs or attention heads and compute variations in model logits. After the interventions,
 1527 the logits drop consistently in all cases, suggesting our jet n -grams indeed can help identify certain
 1528 roles for selected components. Varying impact on logit differences is likely due to overdetermination
 1529 (Mueller, 2024) and our partial selection of jet paths (e.g. for tri-grams we only selected encoding-
 1530 attention-decoding paths, excluding any MLP).

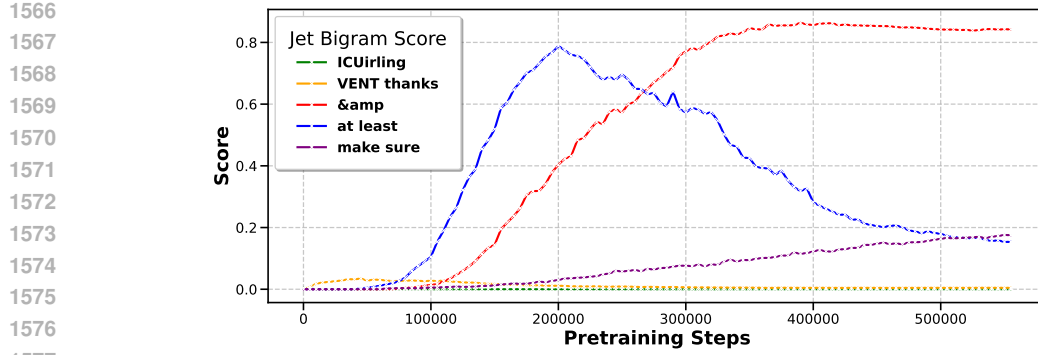
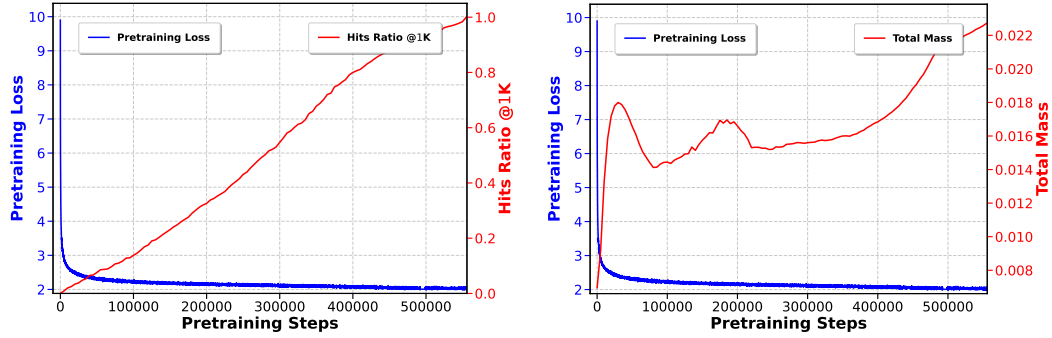
H CASE STUDY 3: TRACING PRETRAINING DYNAMICS WITH JET BI-GRAMS

1531 Pretraining an LLM is usually extremely resource intensive. Therefore it is crucial to monitor the
 1532 progress of a pretraining run to prevent wasting of time and compute. In this section, we show how
 1533 jet bi-grams can serve as an effective signaling tool to trace the pretraining dynamics, providing
 1534 insights about the model’s maturity. Such signals are especially useful to understand what happens
 1535 with the model when the pretraining loss shows marginal improvements and fails to reflect the
 1536 changes inside the model.

1537 **Identifying the top bi-grams.** To assess the model’s progression, we extracted jet bi-grams from
 1538 *OLMo-7B* model checkpoints across 555K pretraining steps. Table 6 presents a summary of the
 1539 top 10 jet bi-grams at different stages of training. Due to space reason, we only show the top 10
 1540 jet bi-grams every 100K steps. Initially, the network exhibits nonsensical jet bi-grams, such as
 1541 “ICUirling”. As training advances, it gradually learns more meaningful combinations, like “at
 1542 least”. This process of acquiring sensible bi-grams stabilizes around step 200K, indicating that
 1543 the model is reaching a level of maturity where the top 10 bi-grams capture common meaning.

1544 **Learning speed.** To evaluate the learning speed of jet bi-grams during pretraining, we consider the
 1545 jet bi-grams at the final training step (555K) as the ground-truth bi-grams. We then chart the hit ratios
 1546 of these ground-truth bi-grams at each pretraining step, as illustrated in Figure 19a. Interestingly,
 1547 even though the pretraining loss (the blue curve) shows only minor improvements after the initial
 1548 50K steps, the model’s acquisition of effective bi-grams continues to progress in a steady, consistent
 1549 manner. Hence bi-grams learning dynamics are active throughout the training procedure, even after
 1550 the training loss stabilizes. This indicates that there is significant behavior change in the model
 1551 which is not well captured by the training loss, an observation that is studied also in grokking and
 1552 double-descent (Zhang et al., 2021; Power et al., 2022). In other words, jet bi-grams may offer
 1553 another point of view for analyzing the learning dynamics compared to pretraining loss. In addition,
 1554 fig. 19b characterizes the total pseudo-joint probability mass of top 1K bi-grams from empirical
 1555 data (Liu et al., 2024). We derive a pseudo-joint jet bi-gram probability using statistical uni-grams
 1556 from (Liu et al., 2024). We observe that the model gradually accumulates probability mass that
 1557 aligns with the real corpus data distribution.

1558 **Learning schemes for different bi-grams.** To understand if there are any differences between the
 1559 learning schemes of different bi-grams, we can trace the progression of the jet bi-gram scores for
 1560 selected bi-grams. Figure 18 provides a visual comparison of how different bi-grams are promoted
 1561 or suppressed during the pretraining process. The different slopes and levels of the lines indicate
 1562 varying rates of learning for the respective bi-grams. We observe that, the model first acquires ran-
 1563 dom bi-grams due to random parameter initialization. These random bi-grams, like “ICUirling”

1578 Figure 18: Visualization of *OLMo-7B*'s promotion and suppression dynamics of jet bi-grams scores.

1590 (a) Top 1K jet bi-gram hit ratios w.r.t. the final step.

1591 (b) Top 1K jet bi-gram mass w.r.t. empirical data.

1592 Figure 19: Analysis of *OLMo-7B*'s pretraining dynamics via measuring its jet bi-gram progression.

1593 and “VENT thanks”, are quickly suppressed in the early steps and never regain high scores. In
 1594 contrast, one-to-many bi-grams like “at least” are first promoted to very high scores but then
 1595 get suppressed perhaps due to the model seeing more of the scope of the token “at”. One-to-one
 1596 bi-grams like “&” (HTML code) are gradually promoted and stabilize. Many-to-many bi-grams
 1597 like “make sure” takes the most time to learn and the scores are still increasing even at the end
 1598 of pretraining. Our findings suggest that the training process effectively promotes certain “good” bi-
 1599 grams, but at different paces, where they might be suppressed later depending on their occurrences
 1600 and linguistic nature. These insights could inform future training strategies, such as targeted training
 1601 on more relevant bi-grams or adjusting the training data to improve the pretraining speed.

1602 Table 6: Bi-gram evolution across pretraining steps for OLMo 7B. Each column represents a distinct step, while
 1603 each row corresponds to a different rank. The table entries are the bi-grams at each step for each rank. The
 1604 number of tokens seen in association with the pretraining steps is also annotated. The model gradually picks
 1605 up meaningful bi-grams after starting from senseless bi-grams (due to random initialization).

Rank	0K OB	[#steps] [#tokens]	100K	200K	300K	400K	555K
0	immortal	's	at least	&	&	&	
1	ICUirling	at least	's	at least	its own	its own	
2	ords architect	its own	&	its own	their own	their own	
3	yaml Adam	okerly	your own	your own	at least	his own	
4	231 next	VENT thanks	its own	their own	your own	make sure	
5	clonal条	iums	iums	more than	his own	your own	
6	Charge{	you're	you're	can't	2nd	2nd	
7	avoir careless	Everything v	2nd	his own	more than	at least	
8	HOLD worsening	erna already	you guys	2nd	make sure	more than	
9	Horse dismant	'my	more than	make sure	can't	iums	